J|A|C|S
ARTICLES
Published on Web 02/01/2003

Biomimetic Aryl Hydroxylation Derived from Alkyl Hydroperoxide at a Nonheme Iron Center. Evidence for an Fe^{IV}=O Oxidant

Michael P. Jensen, Steven J. Lange, Mark P. Mehn, Emily L. Que, and Lawrence Que, Jr.*

Contribution from the Department of Chemistry and Center for Metals in Biocatalysis, University of Minnesota, Minneapolis, Minnesota 55455

Received September 9, 2002; E-mail: que@chem.umn.edu

Abstract: Many nonheme iron-dependent enzymes activate dioxygen to catalyze hydroxylations of arene substrates. Key features of this chemistry have been developed from complexes of a family of tetradentate tripodal ligands obtained by modification of tris(2-pyridylmethyl)amine (TPA) with single α-arene substituents. These included the following: $-C_6H_5$ (i.e., 6-PhTPA), L_1; $-o$-C_6H_4D, o-d_1-L_1; $-C_6D_5$, d_5-L_1; $-m$-$C_6H_4NO_2$, L_2; $-m$-$C_6H_4CF_3$, L_3; $-m$-C_6H_4Cl, L_4; $-m$-$C_6H_4CH_3$, L_5; $-m$-$C_6H_4OCH_3$, L_6; $-p$-$C_6H_4OCH_3$, L_7. Additionally, the corresponding ligand with one α-phenyl and two α-methyl substituents (6,6-Me_2-6-PhTPA, L_8) was also synthesized. Complexes of the formulas $[(L_1)Fe^{II}(NCCH_3)_2](ClO_4)_2$, $[(L_n)Fe^{II}(OTf)_2]$ ($n = 1-7$, OTf = $^-O_3SCF_3$), and $[(L_8)Fe^{II}(OTf)_2]_2$ were obtained and characterized by ^{1}H NMR and UV−visible spectroscopies and by X-ray diffraction in the cases of $[(L_1)Fe^{II}(NCCH_3)_2](ClO_4)_2$, $[(L_6)Fe^{II}(OTf)_2]$, and $[(L_8)Fe^{II}(OTf)_2]_2$. The complexes react with *tert*-butyl hydroperoxide (^{t}BuOOH) in CH_3CN solutions to give iron(III) complexes of *ortho*-hydroxylated ligands. The product complex derived from L_1 was identified as the solvated monomeric complex $[(L_1O^-)Fe^{III}]^{2+}$ in equilibrium with its oxo-bridged dimer $[(L_1O^-)_2Fe^{III}_2(\mu_2\text{-}O)]^{2+}$, which was characterized by X-ray crystallography as the BPh_4^- salt. The L_8 product was also an oxo-bridged dimer, $[(L_8O^-)_2Fe^{III}_2(\mu_2\text{-}O)]^{2+}$. Transient intermediates were observed at low temperature by UV−visible spectroscopy, and these were characterized as iron(III) alkylperoxo complexes by resonance Raman and EPR spectroscopies for L_1 and L_8. $[(L_1)Fe^{II}(OTf)_2]$ gave rise to a mixture of high-spin ($S = 5/2$) and low-spin ($S = 1/2$) Fe^{III}-OOR isomers in acetonitrile, whereas both $[(L_1)Fe(OTf)_2]$ in CH_2Cl_2 and $[(L_8)Fe(OTf)_2]_2$ in acetonitrile afforded only high-spin intermediates. The L_1 and L_8 intermediates both decomposed to form respective phenolate complexes, but their reaction times differed by 3 orders of magnitude. In the case of L_1, ^{18}O isotope labeling indicated that the phenolate oxygen is derived from the terminal peroxide oxygen via a species that can undergo partial exchange with exogenous water. The iron(III) alkylperoxo intermediate is proposed to undergo homolytic O−O bond cleavage to yield an oxoiron(IV) species as an unobserved reactive intermediate in the hydroxylation of the pendant α-aryl substituents. The putative homolytic chemistry was confirmed by using 2-methyl-1-phenyl-2-propyl hydroperoxide (MPPH) as a probe, and the products obtained in the presence and in the absence of air were consistent with formation of alkoxy radical (RO•). Moreover, when one *ortho* position was labeled with deuterium, no selectivity was observed between hydroxylation of the deuterated and normal isotopomeric *ortho* sites, but a significant 1,2-deuterium shift ("NIH shift") occurred. These results provide strong mechanistic evidence for a metal-centered electrophilic oxidant, presumably an oxoiron(IV) complex, in these arene hydroxylations and support participation of such a species in the mechanisms of the nonheme iron- and pterin-dependent aryl amino acid hydroxylases.

Introduction

Metal-mediated oxygen atom transfer to organic substrates is a common mechanistic feature in the enzymology of a broad range of heme and nonheme iron-containing oxygenase enzymes. The former category includes the cytochromes P450, nitric oxide synthases, prostaglandin H synthases, and chloroperoxidases.[1] Among the latter are monometallic α-keto acid- and pterin-dependent hydroxylases[2] and diiron methane monooxygenases.[3] High-valent iron−oxo complexes are invoked as key turnover intermediates and afford two-electron couples, $Fe^{III}/(Fe^{V}$=O or $L^{\bullet,+}Fe^{IV}$=O) for heme, Fe^{II}/Fe^{IV}=O for monometallic nonheme, and $Fe^{III}_2/Fe^{IV}_2O_2$ for bimetallic nonheme enzymes, to accomplish oxo atom transfer. While direct physical evidence for high-valent species has been obtained for heme enzymes[4] and methane monooxygenase,[5] such species have yet to be observed in the catalytic cycles of any mononuclear nonheme iron enzymes.

The aryl amino acid hydroxylases are a family of nonheme, iron(II)-dependent enzymes consisting of three closely related oxidases essential to mammalian physiology, namely phenylalanine (PheH), tyrosine (TyrH), and tryptophan (TrpH) hy-

(1) Sono, M.; Roach, M. P.; Coulter, E. D.; Dawson, J. H. *Chem. Rev.* **1996**, *96*, 2841.

Scheme 1

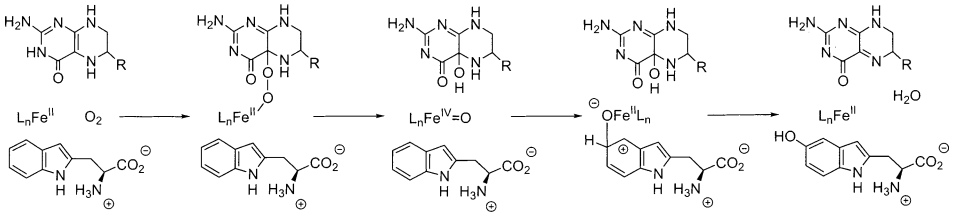

droxylases.[6] The catalytic domain sequences of these enzymes are more than 80% identical, and iron(II), reduced tetrahydrobiopterin (BH_4), and dioxygen are required to selectively hydroxylate the aromatic rings. Crystallographic studies show that the iron(II) center is ligated by a recurring 2-His-1-carboxylate facial triad motif[7] arising from amino acid side chains and water molecules in close proximity to BH_4.[8] Biophysical studies and DFT calculations suggest a reaction mechanism in which iron(II) and BH_4 react with dioxygen to form an iron(II)−peroxo complex, Scheme 1.[9] Heterolysis of the bound O−O bond forms BH_3OH and oxoiron(IV), which reacts as an electrophile toward the aromatic substrate. Release of BH_2, H_2O, and the hydroxylated product completes the turnover. Attention also is called to analogous examples of post-translational oxidative modification of aromatic residues in the vicinity of nonheme iron active sites.[10]

As noted previously, direct evidence for oxoiron(IV) as the hydroxylating intermediate is lacking. However, several observations support this assignment: (i) TyrH $^{16}O/^{18}O$ kinetic isotope effects are consistent with formation of a pterin hydroperoxide from O_2.[11] (ii) Observations of NIH shifts on aryl substrates are indicative of cationic intermediates and are consistent with O-atom transfer.[9,12] (iii) Reaction of deuterated substrate at a truncated TrpH catalytic domain yields an inverse kinetic isotope effect, consistent with partially rate-limiting electrophilic attack.[9] (iv) TyrH and PheH convert 4-CH_3-phenylalanine into a mixture of 3- and 4-methyltyrosines and 4-$HOCH_2$-phenylalanine.[13] (v) Consumption of reduced pterin and O_2 by TyrH can be uncoupled from product formation, indicative of competitive formation of the hydroxylating intermediate.[14] (vi) This competition exhibits a strong substituent effect when 4-substituted phenylalanines are utilized as substrates, which is consistent with an electron-deficient transition state.[13] (vii) The absence of such effects on overall rates of pterin oxidation is consistent with rate-limiting formation of a hydroxylating intermediate prior to actual hydroxylation of the substrates.[15] (viii) A disputed peroxide shunt mode has been reported for TyrH and H_2O_2.[16]

A few reports of model chemistry are relevant to this oxidase enzymology. These include iron-catalyzed oxygenations of coordinated phenolates and arene ligand substituents by O_2/reductant couples.[17,18] Related peroxide-driven reactions also are known.[18−20] However, examinations of the scope and mechanisms of such reactivity remain incomplete.

Our laboratory has utilized iron complexes of tris(2-pyridylmethylamine) (TPA) and related ligands as models of nonheme iron oxygenases and as catalysts for selective oxidative transformations of organic substrates.[21] Such complexes were demonstrated to catalyze hydroxylation of alkanes, epoxidation and *cis*-dihydroxylation of olefins, and sulfoxidation of organic sulfides by peroxides. Evidence has accumulated suggesting these chemistries are mediated by high-valent iron−oxo species,[21,22] including the ability to induce asymmetry in certain products using chiral ligand derivatives.[23] However, the mechanisms of these reactions vary depending on the added

(2) (a) Que, L., Jr.; Ho, R. Y. N. *Chem. Rev*. **1996**, *96*, 2607. (b) Solomon, E. I.; Brunold, T. C.; Davis, M. I.; Kemsley, J. N.; Lee, S.-K.; Lehnert, N.; Neese, F.; Skulan, A. J.; Yang, Y.-S.; Zhou, J. *Chem. Rev.* **2000**, *100*, 235.

(3) (a) Waller, B. J.; Lipscomb, J. D. *Chem. Rev*. **1996**, *96*, 2625. (b) Merkx, M.; Kopp, D. A.; Sazinsky, M. H.; Blazyk, J. L.; Müller, J.; Lippard S. J. *Angew. Chem., Int. Ed.* **2001**, *40*, 2782.

(4) (a) Schlichting, I.; Berendzen, J.; Chu, K.; Stock, A. M.; Maves, S. A.; Benson, D. E.; Sweet, R. M.; Ringe, D.; Petsko, G. A.; Sligar, S. G. *Science* **2000**, *287*, 1615. (b) Kellner, D. G.; Hung, S. C.; Weiss, K. E.; Sligar, S. G. *J. Biol. Chem.* **2002**, *277*, 9641.

(5) (a) Lee, S.-K.; Nesheim, J. C.; Lipscomb, J. D. *J. Biol. Chem*. **1993**, *268*, 21569. (b) Shu, L.; Nesheim, J. C.; Kauffmann, K.; Münck, E.; Lipscomb, J. D.; Que, L., Jr. *Science* **1997**, *275*, 515. (c) Valentine, A. M.; Stahl, S. S.; Lippard, S. J. *J. Am. Chem. Soc.* **1999**, *121*, 3876.

(6) (a) Kappock, T. J.; Carradona, J. P. *Chem. Rev.* **1996**, *96*, 2659. (b) Fitzpatrick, P. F. *Annu. Rev. Biochem*. **1999**, *68*, 355.

(7) Hegg, E. L.; Que, L., Jr. *Eur. J. Biochem*. **1997**, *250*, 625.

(8) (a) Flatmark, T.; Stevens, R. C. *Chem. Rev*. **1999**, *99*, 2137. (b) Que, L., Jr. *Nat. Struct. Biol*. **2000**, *7*, 182.

(9) (a) Moran, G. R.; Derecskei-Kovacs, A.; Hillas, P. J.; Fitzpatrick, P. F. *J. Am. Chem. Soc*. **2000**, *122*, 4535. (b) Bassan, A.; Blomberg, M. R. A.; Siegbahn, P. E. M. *Eur. Chem. J.* **2003**, *9*,,106.

(10) (a) Ormö, M.; deMaré, F.; Regnström, K.; Åberg, A.; Sahlin, M.; Ling, J.; Loehr, T. M.; Sanders-Loehr, J.; Sjöberg, B.-M. *J. Biol. Chem*. **1992**, *267*, 8711. (b) Baldwin, J.; Voegtli, W. C.; Khidekel, N.; Moënne-Loccoz, P.; Krebs, C.; Pereira, A. S.; Ley, B. A.; Huynh, B. H.; Loehr, T. M.; Riggs-Gelasco, P. J.; Rosenzweig, A. C.; Bollinger, J. M., Jr. *J. Am. Chem. Soc*. **2001**, *123*, 7017. (c) Liu, A.; Ho, R. Y. N.; Que, L., Jr.; Ryle, M. J.; Phinney, B. S.; Hausinger, R. P. *J. Am. Chem. Soc.* **2001**, *123*, 5126.

(11) Francisco, W. A.; Tian, G.; Fitzpatrick, P. F.; Klinman, J. P. *J. Am. Chem. Soc*. **1998**, *120*, 4057.

(12) Guroff, G.; Daly, J. W.; Jerina, D. M.; Renson, J.; Witkop, B.; Udenfriend, S. *Science* **1967**, *157*, 1524.

(13) (a) Siegmund, H.-U.; Kaufman, S. *J. Biol. Chem*. **1991**, *266*, 2903. (b) Hillas, P. J.; Fitzpatrick, P. F. *Biochemistry* **1996**, *35*, 6969. (c) Frantom, P. A.; Pongdee, R.; Sulikowski, G. A.; Fitzpatrick, P. F. *J. Am. Chem. Soc*. **2002**, *124*, 4202.

(14) Davis, M. D.; Kaufman, S. *J. Biol. Chem*. **1989**, *264*, 8585.

(15) Fitzpatrick, P. F. *Biochemistry* **1991**, *30*, 6386.

(16) (a) Dix, T. A.; Kuhn, D. M.; Benkovic, S. J. *Biochemistry* **1987**, *26*, 3354. (b) Ribeiro, P.; Pigeon, D.; Kaufman, S. *J. Biol. Chem*. **1991**, *266*, 16207.

(17) (a) Hage, J. P.; Sawyer, D. T. *J. Am. Chem. Soc*. **1995**, *117*, 5617. (b) Funabiki, T.; Yokomizo, T.; Suzuki, S.; Yoshida, S. *Chem. Commun*. **1997**, 151. (c) Hegg, E. L.; Ho, R. Y. N.; Que, L., Jr. *J. Am. Chem. Soc*. **1999**, *121*, 1972.

(18) (a) Ménage, S.; Galey, J.-B.; Hussler, G.; Seité, M.; Fontecave, M. *Angew. Chem., Int. Ed*. **1996**, *35*, 2353. (b) Ménage, S.; Galey, J.-B.; Dumats, J.; Hussler, G.; Seité, M.; Luneau, I. G.; Chottard, G.; Fontecave, M. *J. Am. Chem. Soc*. **1998**, *120*, 13370.

(19) Mekmouche, Y.; Ménage, S.; Toia-Duboc, C.; Fontecave, M.; Galey, J.-B.; Lebrun, C.; Pécaut, J. *Angew. Chem., Int. Ed*. **2001**, *40*, 949.

(20) Kitajima, N.; Ito, M.; Fukui, H.; Moro-oka, Y. *J. Am. Chem. Soc*. **1993**, *115*, 9335.

(21) (a) Leising, R. A.; Norman, R. E.; Que, L., Jr. *Inorg. Chem*. **1990**, *29*, 2553. (b) Leising, R. A.; Brennan, B. A.; Que, L., Jr.; Fox, B. G.; Münck, E. J. *Am. Chem. Soc.* **1991**, *113*, 3988. (c) Kojima, T.; Leising, R. A.; Yan, S.; Que, L., Jr. *J. Am. Chem. Soc*. **1993**, *115*, 11328. (d) Kim, J.; Larka, E.; Wilkinson, E. C.; Que, L., Jr. *Angew. Chem., Int. Ed*. **1995**, *34*, 2048. (e) Kim, J.; Dong, Y.; Larka, E.; Que, L., Jr. *Inorg. Chem*. **1996**, *35*, 2369. (f) Kim, J.; Harrison, R. G.; Kim, C.; Que, L., Jr. *J. Am. Chem. Soc*. **1996**, *118*, 4373. (g) Kim, C.; Chen, K.; Kim, J.; Que, L., Jr. *J. Am. Chem. Soc*. **1997**, *119*, 5964. (h) Chen, K.; Que, L., Jr. *Angew. Chem., Int. Ed*. **1999**, *38*, 2227. (i) Chen, K.; Que, L., Jr. *Chem. Commun*. **1999**, 1375. (j) Costas, M.; Chen, K.; Que, L., Jr. *Coord. Chem. Rev*. **2000**, *200−2*, 517. (k) Miyake, H.; Chen, K.; Lange, S. J.; Que, L., Jr. *Inorg. Chem*. **2001**, *40*, 3534. (l) Chen, K.; Que, L., Jr. *J. Am. Chem. Soc*. **2001**, *123*, 6327. (m) Chen, K.; Costas, M.; Kim, J.; Tipton, A. K.; Que, L., Jr. *J. Am. Chem. Soc*. **2002**, *124*, 3026. (n) Ryu, J. Y.; Kim, J.; Costas, M.; Chen, K.; Nam, W.; Que, L., Jr. *Chem. Commun*. **2002**, 1288.

(22) MacFaul, P. A.; Ingold, K. U.; Wayner, D. D. M.; Que, L., Jr. *J. Am. Chem. Soc*. **1997**, *119*, 10594.

(23) Costas, M.; Tipton, A. K.; Chen, K.; Jo, D.-H.; Que, L., Jr. *J. Am. Chem. Soc*. **2001**, *123*, 6722.

Scheme 2

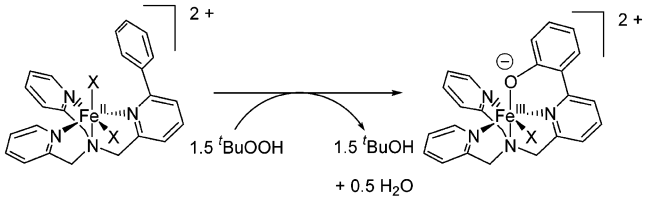

oxidant.[21,22] In the particular case of *tert*-butyl hydroperoxide (^{t}BuOOH), O−O bond homolysis was proposed, leading to *tert*-butoxy radical (^{t}BuO$^\bullet$) and oxoiron(IV).[22] Aliphatic C−H bond hydroxylation then occurs through sequential H-atom abstraction by ^{t}BuO$^\bullet$ and recombination of the alkyl radical at oxoiron(IV), so the metal-centered oxidant is utilized only indirectly. We sought to modify the TPA ligand to introduce a substituent that would react directly with the high-valent species, as observed for 2Cu(I)/O_2,[24] and 2Ni(II)/H_2O_2 couples.[25]

Accordingly, we reported that substitution of an α-phenyl substituent for hydrogen on one pyridyl ring of TPA (e.g., 6-PhTPA, L_1)[26] resulted in an efficient intramolecular *ortho*-hydroxylation when an acetonitrile solution of the complex salt [(6-PhTPA)$Fe^{II}(NCCH_3)_2$]$(ClO_4)_2$ is treated with ^{t}BuOOH, Scheme 2.[27] This reaction bears a strong resemblance to that afforded by PheH and can be considered a model for the unknown peroxide shunt. We have since broadened the chemistry of Scheme 2 to include the range of aryl substituents summarized in Scheme 3. Methyl substituents also were added to the other pyridine arms to control the donor properties of the ligand and the spin state of the iron.[28] This paper describes the syntheses of Fe(II) complexes of this ligand range and reactivity of the solvated cations (i.e., $[(L)Fe^{II}(NCCH_3)_2]^{2+}$) with ^{t}BuOOH, including spectroscopic detection of reaction intermediates and characterization of product complexes (i.e., $[(LO^-)Fe^{III}(NCCH_3)]^{2+}$) and free phenol ligands (i.e., LOH). These results are intended to support further quantitative kinetic and mechanistic investigation of the hydroxylation reaction.[29]

Experimental Section

Materials. All materials used were ACS reagent grade or better and were used as received, except for drying and degassing of bulk solvents by routine methods as required. NMR solvents were used as received from Cambridge Isotope Labs. Aryl boronic acids were purchased from Aldrich and Lancaster. $Pd(PPh_3)_4$ was purchased from Lancaster. Bis-(2-pyridylmethyl) amine was purchased from Richman Chemicals.

Scheme 3

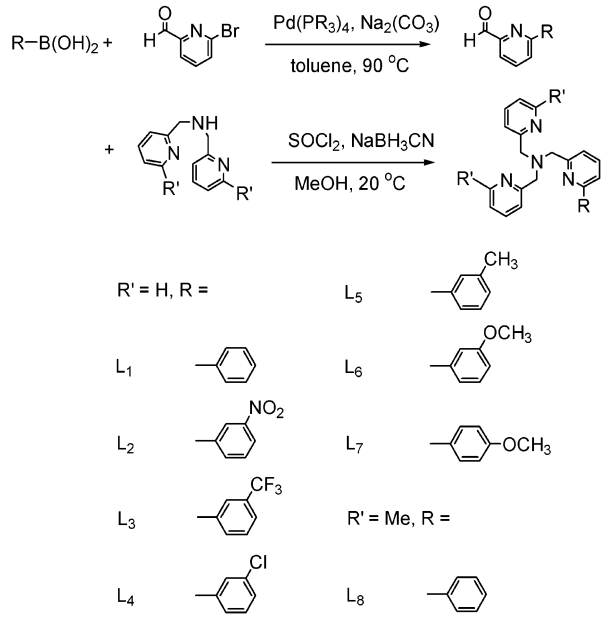

2-Methyl-1-phenyl-2-propyl hydroperoxide (MPPH),[30] bis(6-methyl-2-pyridylmethyl)amine,[31] 6-bromo-2-pyridinecarboxaldehyde,[32] *ortho*-d_1-bromobenzene,[33] and $Fe(OTf)_2$·$2CH_3CN$[34] were synthesized by literature procedures. All other reagents were purchased from Aldrich.

Ligand Syntheses. The preparation of the *ortho*-d_1 isotopomer of L_1 (*o*-d_1-L_1) is described below and outlined in Scheme 3. Other ligands were obtained in an identical manner by substitution of the appropriate aryl boronic acid (L_1−L_8) or bis(6-methyl-2-pyridylmethyl)amine (L_8). The ligands were characterized by ^{1}H NMR spectroscopy (vide infra) and were free of observable impurities except for trace amounts of 6-aryl-2-pyridylcarbinols in some cases.

Preparation of *o*-d_1-L_1 (6-*o*-d_1-PhTPA). An aliquot of *o*-d_1-bromobenzene (4.00 g, 25.3 mmol) was dissolved in dry THF (50 mL) in a three-neck flask equipped with a gas inlet and a dropping funnel. The solution was cooled to −78 °C under a constant purge of dry argon gas. An aliquot (20 mL) of a ^{n}BuLi solution (1.6 M in hexane) was transferred by cannula into the dropping funnel and slowly added over 5 min into the cold reaction solution. After the solution was stirred for 1 h, $B(OMe)_3$ (4.00 mL, 36 mmol) was added, and the new solution was allowed to warm gradually to room temperature overnight. To the white suspension was cautiously added 1.0 M HCl (50 mL). After the mixture was stirred for 1 h, the aqueous layer was separated and extracted with CH_2Cl_2 (2 × 50 mL). The extracts were combined with the organic layer, washed with water, and dried over Na_2SO_4. Removal of solvent by rotary evaporation yielded crude *o*-d_1-phenylboronic acid (1.87 g, 15.2 mmol, 60%). A sample of 6-bromo-2-pyridinecarboxaldehyde (2.05 g, 11.0 mmol) was dissolved in toluene (15 mL) in a three-neck flask capped with a gas inlet, a condenser with a gas outlet to a bubbler, and a glass stopper. The reaction apparatus was flushed with argon. $Pd(PPh_3)_4$ (0.30 g, 0.3 mmol) was suspended in anaerobic toluene (5 mL), and the suspension was added to the reaction flask against an active argon purge, followed by aqueous 2.0 M Na_2CO_3 (10 mL) and the crude o-d_1-phenylboronic acid dissolved in methanol (8 mL). The flask was capped, and the suspension was heated to reflux for 10 h. A 2.0 M aqueous solution of $Na_2(CO_3)$ (40 mL) and CH_2Cl_2 (100 mL) were added to the cooled solution. The aqueous phase was separated and extracted with fresh CH_2Cl_2 (1 × 25 mL), and the

(24) (a) Karlin, K. D.; Hayes, J. C.; Gultneh, Y.; Cruse, R. W.; McKown, J. W.; Hutchinson, J. P.; Zubieta, J. *J. Am. Chem. Soc.* **1984**, *106*, 2121. (b) Karlin, K. D.; Nasir, M. S.; Cohen, B. I.; Cruse, R. W.; Kaderli, S.; Zuberbuehler, A. D. *J. Am. Chem. Soc.* **1994**, *116*, 1324. (c) Itoh, S.; Kondo, T.; Komatsu, M.; Ohshiro, Y.; Li, C.; Kanehisa, N.; Kai, Y.; Fukuzumi, S. *J. Am. Chem. Soc.* **1995**, *117*, 4714. (d) Itoh, S.; Nakao, H.; Berreau, L. M.; Kondo, T.; Komatsu, M.; Fukuzumi, S. *J. Am. Chem. Soc.* **1998**, *120*, 2890 and references therein. (e) Holland, P. L.; Rodgers, K. R.; Tolman, W. B. *Angew. Chem., Int. Ed.* **1999**, *38*, 1139 and references therein. (f) Itoh, S.; Taki, M.; Nakao, H.; Holland, P. L.; Tolman, W. B.; Que, L., Jr.; Fukuzumi, S. *Angew. Chem., Int. Ed.* **2000**, *39*, 398. (g) Hayashi, H.; Uozumi, K.; Fujinami, S.; Nagatomo, S.; Shiren, K.; Furutachi, H.; Suzuki, M.; Uehara, A.; Kitagawa, T. *Chem. Lett.* **2002**, 416.
(25) (a) Itoh, S.; Bandoh, H.; Nagatomo, S.; Kitagawa, T.; Fukuzumi, S. *J. Am. Chem. Soc.* **1999**, *121*, 8945. (b) Shiren, K.; Ogo, S.; Fujinami, S.; Hayashi, H.; Suzuki, M.; Uehara, A.; Watanabe, Y.; Moro-oka, Y. *J. Am. Chem. Soc.* **2000**, *122*, 254. (c) Itoh, S.; Bandoh, H.; Nakagawa, M.; Nagatomo, S.; Kitagawa, T.; Karlin, K. D.; Fukuzumi, S. *J. Am. Chem. Soc.* **2001**, *123*, 11168.
(26) Chuang, C.-L.; Lim, K.; Canary, J. W. *Supramol. Chem.* **1995**, *5*, 39.
(27) Lange, S. J.; Miyake, H.; Que, L., Jr. *J. Am. Chem. Soc.* **1999**, *121*, 6330.
(28) Zang, Y.; Kim, J.; Dong, Y.; Wilkinson, E. C.; Appelman, E. H.; Que, L., Jr. *J. Am. Chem. Soc.* **1997**, *119*, 4197.
(29) Jensen, M. P.; Que, L., Jr. Unpublished results.
(30) Arends, I. W. C. E.; Ingold, K. U.; Wayner, D. D. M. *J. Am. Chem. Soc.* **1995**, *117*, 4710.
(31) Da Mota, M. M.; Rogers, J.; Nelson, S. M. *J. Chem. Soc. A* **1969**, 2036.
(32) Cai, D.; Hughes, D. L.; Verhoeven, T. R. *Tetrahedron Lett.* **1996**, *37*, 2537.
(33) Renaud, R. N.; Kovachic, D.; Leitch, L. C. *Can. J. Chem.* **1961**, *39*, 21.
(34) Hagen, K. S. *Inorg. Chem.* **2000**, *39*, 5867.

combined organic extracts were dried overnight (Na_2SO_4). A major product was revealed by TLC on silica (4:1 v:v CH_2Cl_2−toluene) at R_f 0.59 (vs 0.49 for 2- bromo-6-pyridinecarboxaldehyde). 6-*o*-d_1-Phenyl-2-pyridinecarboxyaldehyde was obtained following column chromatography on silica (1:1 v:v CH_2Cl_2−toluene) as a pale yellow oil (1.38 g, 7.5 mmol, 68% vs 6-bromo-2-pyridinecarboxaldehyde, 49% vs deuterium). Successful separation of 6-*o*-d_1-phenyl-2-pyridinecarboxaldehyde was indicated by appearance in a ^{1}H NMR spectrum ($CDCl_3$) of a single aldehyde resonance at 10.17 ppm, compared to 6-bromo-2-pyridinecarboxaldehyde at 9.98 ppm.

A solution of bis(2-pyridylmethyl)amine (1.65 g, 8.3 mmol) dissolved in dry methanol (25 mL) was added to the 6-*o*-d_1-phenyl-2-pyridinecarboxaldehyde. Thionyl chloride (300 μL) was added with care to the stirred yellow solution. The flask was capped, and the solution was stirred 2.0 h before solid $NaBH_3CN$ (1.19 g, 18.9 mmol) and a purge needle were added. The solution was stirred an additional 3.0 h, and the reaction was quenched by dropwise addition of 12 M HCl. After gas evolution ceased, the solution was concentrated to a yellow slurry by rotary evaporation, to which water (20 mL) was added. The solution was washed with ether (2 × 30 mL), and concentrated NH_4OH was added until the solution was basic. The product was extracted into diethyl ether (3 × 25 mL), and the combined extracts were dried over Na_2SO_4. The dried solution was concentrated by rotary evaporation and eluted from a column of neutral alumina (3 cm diameter × 30 cm length) with 50:1 v:v CH_2Cl_2−CH_3OH to give the product as a pale yellow oil, 1.49 g (4.1 mmol, 55%), which crystallized on standing. Analysis of the product ligand by mass spectrometry was consistent with incorporation of 0.97(1) equiv of deuterium. ^{1}H NMR (δ, ppm in $CDCl_3$): 8.54 (2H, ddd, 4.9, 1.4 and 1.4 Hz, α); 8.03 (1H, 7.5 Hz, H_o); 7.73 (1H, dd, 7.5 and 7.5 Hz, γ'); 7.69−7.61 (4H, m, β, γ); 7.60 (1H, d, 7.0 Hz, β'); 7.50 (1H, d, 7.0 Hz, β'); 7.47 (2H, m, H_m); 7.40 (1H, t, 7.0 Hz, H_p); 7.17 (2H, dd, 8.0 and 4.9 Hz, β); 4.03 (6H, br s, −NCH_2−). ^{2}H NMR (δ, ppm in $CHCl_3$): 8.1 (*ortho*).

Independent Synthesis of 6-*ortho*-HOC$_6$H$_4$-TPA, L$_1$OH. A sample of 6-*ortho*-$CH_3OC_6H_4$-TPA was obtained by the procedure described above using *ortho*-methoxyphenylboronic acid and was characterized by ^{1}H NMR spectroscopy (δ, ppm in $CDCl_3$): 8.54 (2H, d, 5.0 Hz, α); 7.83 (1H, d, 7.0 Hz, H_o); 7.64−7.74 (6H, m, β, γ, β', γ'); 7.49 (1H, d, 8.0 Hz, β'); 7.36 (1H, ddd, 8.0, 7.5 and 2.0 Hz, H_p); 7.16 (2H, ddd, 6.0, 6.0 and 1.5 Hz, β); 7.07 (1H, ddd, 7.5, 7.5 and 1.0 Hz, H_m); 6.99 (1H, d, 8.0 Hz, H_m'); 4.1 (6H, br s, −NCH_2−); 3.84 (3H, s, −OCH_3). Solid NaSEt (1.2 g, 11.4 mmol) was added to a solution of the product (0.76 g, 1.92 mmol) in DMF. The slurry was heated to reflux for 3 h and then allowed to cool. The yellow solution was poured into water, and the mixture was acidified with 12 M HCl (10 mL). The aqueous solution was washed with CH_2Cl_2 (3 × 50 mL) and cautiously neutralized with sodium bicarbonate. The product was extracted into CH_2Cl_2 (3 × 50 mL), and the combined extracts were washed with water (3 × 50 mL) and dried over $MgSO_4$. The product was recovered as a yellow oil in 85% yield following column chromatography on alumina ($CHCl_3$−MeOH). ^{1}H NMR spectroscopy (δ, ppm in $CDCl_3$): 8.55 (2H, d, 5.0 Hz, α); 7.79−7.69 (7H, m, H_o, β, γ, β', γ'); 7.45 (1H, d, 6.0 Hz, β'); 7.32 (1H, ddd, 8.5, 7.0 and 1.8 Hz, H_p); 7.20 (2H, ddd, 6.0, 5.0 and 2.0 Hz, β); 7.04 (1H, dd, 8.5 and 1.2 Hz, H_m'); 6.90 (1H, ddd, 8.0, 7.0 and 1.0 Hz, H_m); 4.03 (4H, s, −NCH_2−); 3.99 (2H, s, −NCH_2−).

Preparation of Iron(II) Complexes. Iron(II) complexes were synthesized as described below with formulas $[(L_1)Fe^{II}(NCCH_3)_2](ClO_4)_2$,[27] $[(L_n)Fe^{II}(OTf)_2]$ ($OTf^- = {}^-O_3SCF_3$, triflate) for L_1−L_7, and $[(L_8)Fe^{II}(OTf)_2]_2$. **Caution**! *Perchlorate salts of organic cations are potentially explosive*.[35] While no difficulties were encountered in the work described here, functionally identical triflate complexes were also obtained (vide infra).

[(*o*-*d*$_1$-L$_1$)Fe^{II}(NCCH$_3$)$_2$](ClO$_4$)$_2$. Crystals of 6-*o*-d_1-PhTPA (*o*-d_1-L_1, 0.225 g, 0.61 mmol) were dissolved in CH_3CN (5 mL) under a N_2 atmosphere. A solid sample of $Fe(ClO_4)_2 \cdot nH_2O$ (0.190 g, 0.47 mmol, $n = 8.3$) was added, and the yellow-green solution was stirred for 30 min. The reaction solution was poured onto Na_2SO_4 and stirred 2.0 h. The solution was decanted and filtered twice. Dry ether (ca. 20 mL) was added until the solution was persistently cloudy, and the solution was allowed to stand overnight at ambient temperature. The product crystallized as yellow-green rhombic plates, which were washed with ether and dried to constant mass, 0.228 g (69%). Additional ether was added to the concentrated mother liquor and a second crop was obtained, 0.060 g (18%). Anal. Calcd (found) for $C_{28}H_{27}DCl_2FeN_6O_8$: C, 47.75 (47.50); H, 4.01 (4.00); N, 11.93 (11.91).

[(*d*$_5$-L$_1$)Fe^{II}(NCCH$_3$)$_2$](ClO$_4$)$_2$. The complex was prepared as described above using 6-d_5-PhTPA [d_5-L_1, ^{2}H NMR (δ, ppm in $CHCl_3$): 8.0 (2D, *ortho*); 7.5 (3D, *para* + *meta*)] and was isolated in two crops in 70% combined yield. Anal. Calcd (found) for $C_{28}H_{23}D_5Cl_2FeN_6O_8$: C, 47.48 (47.37); H, 3.98 (3.99); N, 11.87 (11.86).

[(L$_1$)Fe^{II}(NCCH$_3$)$_2$](ClO$_4$)$_2$. The complex was prepared as described above using 6-PhTPA (L_1) and isolated as one crop in 70% yield. Anal. Calcd (found) for $C_{28}H_{28}Cl_2FeN_6O_8$: C, 47.82 (47.51); H, 4.01 (3.98); N, 11.95 (11.46). $E_{1/2} = +1240$ mV vs SCE ($\Delta E = 70$ mV, $i_{pc}/i_{pa} = 0.71$).

[(L$_1$)Fe^{II}(OTf)$_2$]. Crystals of 6-PhTPA (L_1, 0.150 g, 0.41 mmol) and a solid sample of $Fe(OTf)_2 \cdot 2CH_3CN$ (0.175 g, 0.40 mmol) were dissolved in THF (5 mL) under a N_2 atmosphere, and the resulting pale yellow solution was stirred for 60 min. The reaction solution was taken to dryness under vacuum, and the yellow oil was extracted into CH_2Cl_2. This was repeated once, and then CH_2Cl_2 (4 mL) was added to the oil and a minimum volume of THF was added to obtain a homogeneous solution. The solution was layered with hexane (12 mL) to produce yellow needlelike crystals on standing overnight. The mother liquor was decanted, and the crystals were washed with hexane and dried to constant mass, 0.256 g (88%). Anal. Calcd (found) for $C_{26}H_{22}F_6FeN_4O_6S_2 \cdot H_2O$: C, 42.29 (42.55); H, 3.28 (3.21); N, 7.59 (7.56); F, 15.44 (15.41).

[(L$_2$)Fe^{II}(OTf)$_2$]. The complex was prepared as described for L_1 above and isolated as yellow crystals in 78% yield. Anal. Calcd (found) for $C_{26}H_{21}F_6FeN_5O_8S_2$: C, 40.80 (41.12); H, 2.77 (2.89); N, 9.15 (8.97); F, 14.89 (14.73). $E_{1/2} = +1240$ V vs SCE ($\Delta E = 70$ mV, $i_{pc}/i_{pa} = 0.66$). $E_{pc} = -1010$, −1160 mV vs SCE (irreversible).

[(L$_3$)Fe^{II}(OTf)$_2$]. The complex was prepared as described above and isolated as yellow crystals in 47% yield. Anal. Calcd (found) for $C_{27}H_{21}F_9FeN_4O_6S_2 \cdot H_2O$: C, 40.21 (40.24); H, 2.87 (2.90); N, 6.95 (6.82); F, 21.20 (21.43).

[(L$_4$)Fe^{II}(OTf)$_2$]. The complex was prepared as described above and isolated as yellow crystals in 50% yield. Anal. Calcd (found) for $C_{26}H_{21}ClF_6FeN_4O_6S_2$: C, 41.37 (41.43); H, 2.80 (2.71); N, 7.42 (7.32); F, 15.10 (14.76).

[(L$_5$)Fe^{II}(OTf)$_2$]. The complex was prepared as described above and isolated as yellow crystals in 11% yield. Anal. Calcd (found) for $C_{27}H_{24}F_6FeN_4O_6S_2 \cdot H_2O$: C, 43.10 (43.44); H, 3.48 (3.41); N, 7.45 (7.44); F, 15.15 (15.16).

[(L$_6$)Fe^{II}(OTf)$_2$]. The complex was prepared as described above and isolated as yellow crystals in 33% yield. Anal. Calcd (found) for $C_{27}H_{24}F_6FeN_4O_7S_2$: C, 43.21 (43.35); H, 3.22 (3.25); N, 7.47 (7.47); F, 15.19 (15.40).

[(L$_7$)Fe^{II}(OTf)$_2$]. The complex was prepared as described above and isolated as yellow crystals in 98% yield. Anal. Calcd (found) for $C_{27}H_{24}F_6FeN_4O_7S_2$: C, 43.21 (42.91); H, 3.22 (3.31); N, 7.47 (7.29). $E_{1/2} = +1210$ mV vs SCE ($\Delta E = 74$ mV, $i_{pc}/i_{pa} = 0.72$).

[(L$_8$)Fe^{II}(OTf)$_2$]$_2$. The complex was prepared as described above and isolated as white crystals in 48% yield. Anal. Calcd (found) for $C_{56}H_{52}F_{12}Fe_2N_8O_{12}S_4 \cdot 0.5CH_2Cl_2$: C, 44.08 (43.97); H, 3.47 (3.66); N, 7.26 (7.18); F, 14.81 (14.45). $E_{pa} = +1440$, 1630 mV vs SCE (irreversible).

(35) (a) Wolsey, W. C. *J. Chem. Educ.* **1973**, *50*, A335. (b) Raymond, K. N. *Chem. Eng. News* **1983**, *61*, 1 (December 5), 4.

Reactivity Studies of Complexes with ^{t}BuOOH. In a typical experiment, 5.0 μmol of complex (e.g., 3.5 mg of $[(L_1)Fe(NCCH_3)_2](ClO_4)_2$) was dissolved in dry acetonitrile (5.00 mL) under N_2 to give a pale yellow-green solution of the solvento complex with the general formula $[(L)Fe^{II}(NCCH_3)_2](X)_2$ (X = OTf^-, ClO_4^-). This solution was transferred to a cuvette and sealed under N_2 with a rubber septum. The cuvette was placed in a cryogenic cell holder on a UV−visible spectrophotometer and cooled to the desired reaction temperature. An aliquot of dry ^{t}BuOOH (5.5 M in nonane) was diluted with dry CH_3CN to a concentration of 150 mM on the benchtop. This stock solution (120 μL) was injected through the septum to initiate the reaction. Thus, initial concentrations were 1.0 ± 0.1 mM complex and 3.5 ± 0.5 mM peroxide. The reaction was monitored to completion, and the solution was warmed to room temperature and diluted with water (5.0 mL). Some 12 M HCl was added dropwise until the color was completely bleached. The pale yellow solution was washed with ether, and concentrated NH_4OH was added until the solution was alkaline. The solution was extracted with ether (2 × 5 mL), and the extracts were washed with water (2 × 5 mL). The extracts were dried under vacuum, and the white residue was taken up into $CDCl_3$ and characterized by ^{1}H NMR spectroscopy (vide infra). Integration against a known quantity of added 2,6-*tert*-butyl-4-methylphenol was used to quantify the ligand recovery. A portion of the $CDCl_3$ solution was diluted with CH_3CN and analyzed by electrospray mass spectrometry.

NIH Shift Analysis. Product ligand from reaction of *o*-d_1-L_1 was extracted into $CDCl_3$ and characterized by ^{1}H NMR spectroscopy as described above. Curve fittings (Lorentzian functions) carried out using Grams/32 Spectral Notebase Version 4.04 (Galactic) gave the relative areas of the overlapping doublet and doublet of doublet $^3J_{HH}$ coupling patterns for the H_m and H_p resonances, which indicated the ratio of deuterons to protons in the adjacent H_o and H_m' positions, respectively. The fits were simplified by use of selective homonuclear decoupling to collapse $^4J_{HH}$ multiplicity. Total deuterium retention was confirmed by mass spectrometry. The data were corrected for product derived from residual d_0-L_1 (3%).

MPPH Product Analysis. Reactions were conducted as described for ^{t}BuOOH above. Reaction solutions were saturated with O_2 by bubbling the pure gas from a balloon through a purge needle for a period of 20−30 s just prior to addition of the MPPH stock solution. The product solutions were diluted with a stock solution of naphthalene in CH_3CN to known concentrations and then passed through silica gel to remove iron complexes. These solutions were analyzed by gas chromatography. Controls were run to obtain retention times for CH_3CN solutions of authentic bibenzyl, benzyl alcohol, benzaldehyde, and 2-methyl-1-phenyl-2-propyl alcohol and to calibrate the detector response against the internal naphthalene standard.

Base Titration of $[(L_1O^-)Fe^{III}(OH_2)]^{2+}$. A ^{t}BuOOH stock solution was prepared by adding an aliquot (60 μL) of 70 wt % aqueous solution to dry CH_3CN (2.00 mL). To a cold (233 K) solution of $[(L_1)Fe^{II}(NCCH_3)_2](ClO_4)_2$ (6.3 mg) in CH_3CN (9.73 mL) was added a 130 μL aliquot of peroxide stock solution to give a reaction solution with $[complex]_0 = 0.9$ mM, $[^tBuOOH]_0 = 2.8$ mM, and $[H_2O] > 6$ mM. After completion of the reaction, an aliquot (3.50 mL) of the violet solution was placed in a cuvette maintained at 293 K. A stock solution (71 mM) of NEt_3 (49 μL) was prepared in CH_3CN (4.91 mL); this was added to the complex solution in 5.0 μL (ca. 0.1 mM) aliquots, and a UV−visible spectrum was recorded after each addition. Accumulation of $[(L_1O^-)_2Fe^{III}_2(\mu\text{-}O)]^{2+}$ was indicated by a gradual color change to orange and development of an absorption maximum at 486 nm. A Job's law plot indicated conversion to the dimeric complex was complete upon addition of 0.9 ± 0.2 equiv of NEt_3. The color change was reversed by addition of $HClO_4$.

Isolation of $[(L_1O^-)_2Fe^{III}_2(\mu\text{-}O)](BPh_4)_2$.[27] To a rapidly stirred solution of $[(L_1)Fe^{II}(NCCH_3)_2](ClO_4)_2$ (30 mg, 43 μmoles) in CH_3CN (25 mL) was added ^{t}BuOOH (3.0 equiv) by syringe pump under an N_2 atmosphere. To the blue solution was added NEt_3 until the solution was orange and no further changes were observed in UV−visible spectra. The solvent was taken to dryness under vacuum, and the pasty orange solids were washed with ether. Addition of solid $NaBPh_4$ to MeOH extracts induced precipitation of an orange powder in ca. 65% yield, which was recrystallized from MeOH/DMF. Anal. Calcd (found) for $C_{96}H_{82}B_2Fe_2N_8O_3{\cdot}CH_3OH$: C, 74.63 (74.86); H, 5.55 (5.47); N, 7.18 (7.40).

X-ray Crystallographic Studies. Data collections and structure solutions were conducted at the X-ray crystallographic facility of the Department of Chemistry at the University of Minnesota. All calculations were performed using SGI INDY R4400-SC or Pentium computers using the current SHELXTL suite of programs.[36] Suitable crystals were identified and placed onto the tips of 0.1 mm glass capillaries and mounted on a Bruker SMART system for data collection at 173(2) K. Preliminary unit cells were calculated from three sets of 20 frames oriented so orthogonal wedges of reciprocal space were surveyed. Final cell constants were calculated from the full set of strong reflections of the data collection. Data were collected using graphite-monochromated Mo Kα radiation with a frame time of 30 s and a detector distance of 4.9 cm. A randomly oriented region of reciprocal space was surveyed to the extent of 1.3−1.5 hemispheres to a resolution of 0.84 Å. Three major swaths of frames were collected with 0.30° steps in ω at three different ϕ settings and a detector position of −28° in 2θ. Collected data were corrected for absorption and decay (SADABS).[37] In the event the unit cell was triclinic, additional sets of frames were collected to better model the absorption correction.

Space groups were assigned on the basis of systematic absences and intensity statistics. Structures were solved by direct methods. All non-hydrogen atoms were located in difference Fourier maps and submitted to full-matrix least-squares refinement with anisotropic displacement parameters. All hydrogen atoms were placed in idealized positions and refined as riding atoms with relative isotropic displacement parameters. Additional details are given in Tables 1 and 2 and below.

$[(L_1)Fe^{II}(NCCH_3)_2](ClO_4)_2$.[27] One perchlorate anion was disordered over two overlapping, partially occupied positions. A total of 182 restraints were applied (SHELXTL SAME, and DELU) to this and the other perchlorate to achieve the best model possible. The chlorine U_{ij} values were made identical with the SHELXTL constraint EADP due to the near overlap. The partial occupancies were found essentially to have a 0.50:0.50 ratio.

$[(L_1O^-)_2Fe^{III}_2(\mu\text{-}O)](BPh_4)_2$.[27] The bridging oxygen atom was located on the crystallographic inversion center, so each asymmetric unit consisted of half the cation.

$[(L_8)Fe^{II}(OTf)_2]{\cdot}CH_2Cl_2$. Only half of the dimer complex is unique. The CH_2Cl_2 molecule was disordered over two positions (71:29) and over the inversion center (50:50). The C14 methyl group was best modeled as rotationally disordered.

Other Physical Methods. ^{1}H NMR spectra (499.87 MHz) were recorded on a Varian VI-500 Unity-plus spectrometer and referenced to residual solvent ($CHCl_3$ = 7.26 ppm, CHD_2CN = 1.94 ppm). ^{2}H NMR spectra (46.03 MHz) were recorded on a Varian VXR-300 Unity-plus spectrometer and referenced to solvent ($CDCl_3$ = 7.26 ppm). ^{19}F NMR spectra (282.15 MHz) were recorded on a Varian VI-300 spectrometer and referenced to external $CFCl_3$ (0.00 ppm). UV−visible spectra were recorded over a 300−900 nm range on a Hewlett-Packard 8453 diode-array spectrophotometer. Low observation temperatures were obtained using a dewar fitted with quartz windows, through which a closed loop of methanol was pumped from a circulating bath (Neslab) equipped with an immersion cooler (Neslab Cryocool CC100-II) under control of a thermostat. X-band EPR spectra were obtained at 1.8 K on a Bruker E-500 spectrometer equipped with an Oxford ESR-10 liquid-helium cryostat. The magnetic field was calibrated with a gaussmeter, and the microwave frequency was determined with a

(36) *SHELXTL-Plus*, v. 5.10; Bruker Analytical X-ray Systems: Madison, WI.
(37) R. Blessing, *Acta Crystallogr. A* **1995**, *51*, 33.

counter. Resonance Raman spectra were recorded at 4 cm^{-1} resolution on an Acton AM-506 spectrophotometer using a Kaiser Optical holographic super-notch filter with a Princeton Instruments CCD detector cooled with liquid nitrogen. Data were collected using a backscattering geometry on frozen CH_3CN samples using 514.5, 568.2, or 632.8 nm radiation from a 375B CW dye laser (rhodamine 6G) pumped by a Spectra Physics 2030-15 Ar ion laser. Mass spectra were obtained either by fast atom bombardment (FAB, LSIMS) ionization from *m*-nitrobenzyl alcohol matrixes on a VG 7070E-HF spectrometer or from CH_3CN solutions by electrospray ionization on a Thermo Finnigan LCQ spectrometer. Cyclic voltammetric analyses of selected Fe(II) complexes were carried out using a CS-100 electrochemical analyzer (Cypress Systems, Inc., Lawrence, KS) interfaced to a three-electrode system (glassy carbon working, Pt wire counter, Ag wire reference electrodes). Measurements were made from 2.0 mM analyte solutions in dry acetonitrile in the presence of 0.10 M NBu_4ClO_4 as supporting electrolyte. Potentials were referenced internally to the ferrocene couple (+380 mV vs SCE).[38] Elemental analyses were performed by Atlantic Microlabs, Inc. (Norcross, GA).

Results

Syntheses and ^{1}H NMR Characterization of Ligands. The ligands used in this study, and their syntheses are summarized in Scheme 3. The approach was characterized by significant flexibility and generality and was applicable to a broad range of ligands. Thus, the aryl substituents were introduced onto 6-bromo-2-pyridinecarboxaldehyde by catalytic Suzuki coupling,[39] and bis(2-pyridylmethyl)amines were added subsequently across the aldehyde in a reductive amination.[40] In principle, the synthetic scheme could be simplified further by reversing the order of the steps, i.e., coupling aryl boronic acids to a common 6-bromo-TPA intermediate.[41] However, purification of coupling products proved to be easier to achieve and verify with the pyridinecarboxaldehydes, so the longer approach was adopted.

The series of ligands depicted in Scheme 3 was intended to introduce a range of α-aryl substituents with modified susceptibility to electrophilic aromatic substitution at the *ortho* carbons. Accordingly, a series of functional groups ($-NO_2$, $-CF_3$, $-Cl$, $-CH_3$, $-OCH_3$) was placed at one *meta* position to give L_2-L_6 derivatives of 6-PhTPA, L_1. Substituents placed in this position were expected to exert significant electronic effects on the *ortho* carbons, while minimizing electronic and steric effects on the *ipso* pyridine and the chelated metal ion.

Comparison of ^{1}H NMR spectra of the substituted ligands (Table S1) indicated the efficacy of this approach. A set of resonances common to all the ligands (L_1-L_7) was observed in $CDCl_3$ solutions for the six methylene protons and the unsubstituted pyridines. The remaining signals were affected by the introduced substituents. Resonances of the unsubstituted arene of L_1 appeared at 8.01 ppm (*ortho*), 7.49 ppm (*meta*), and 7.40 ppm (*para*); these resonances were absent in the spectrum of d_5-L_1, and the assignments based on *J*-couplings were confirmed by the COSY technique. As expected, the *ortho* and *para* proton resonances were strongly deshielded by electron-withdrawing *meta* substitutents, varying over a more than 1.3 ppm range between L_2 and L_6, while the remaining *meta* proton and the *ipso* pyridine protons were scarcely affected. The latter point was illustrated by comparison of the *ipso* pyridine resonances, which were coincident among L_1-L_6 to within 0.1 ppm. In contrast, *para* substitution induced comparable effects within the pyridine, even though the *ortho* protons were essentially unaffected.

Hence, the NMR data supported the expectation that *meta* substitution affords gross manipulation of electronic properties at the *ortho* carbons without significant perturbation of the chelating properties of the ligand. This point was reflected further by the electrochemical behaviors of Fe(II)/Fe(III) redox couples supported by L_1, L_2, and L_7. Quasi-reversible couples were observed at essentially coincident potentials for these three ligand complexes by cyclic voltammetry, notwithstanding the effects of the most electron-withdrawing (L_2, + 1240 mV vs SCE) and electron releasing (L_7, + 1210 mV) aryl substituents in comparison to the parent complex (L_1, + 1240 mV).

A second class of ligand modification encompassed by Scheme 3 was the substitution of methyl groups for hydrogen at the α-pyridine position, L_8 vs. L_1. This modification has been demonstrated to disfavor low spin states of coordinated iron ions, presumably by reducing the ligand field strength through steric repulsion with the metal center.[28] Resonances of the pyridine ring protons of L_8 were significantly convoluted, but the phenyl ring resonances were comparable to those of L_1 and a characteristic α-methyl resonance was observed at 2.53 ppm.

Iron(II) Complexes. Homogeneous solutions of Fe(II) ligand complexes were obtained simply by dissolving a 1:1 mixture of ligands and Fe(II) salts. A yellow-green crystalline complex salt $[(L_1)Fe^{II}(NCCH_3)_2](ClO_4)_2$ was obtained in good yield from CH_3CN/Et_2O, but this approach failed with other ligands. Alternatively, use of $Fe^{II}(OTf)_2 \cdot 2CH_3CN$ in THF generally afforded bright yellow crystals of neutral complexes $[(L_n)Fe^{II}(OTf)_2]$ from CH_2Cl_2/*n*-hexane for L_1-L_7, as well as colorless crystals of $[(L_8)Fe^{II}(OTf)_2]_2$. These dissolved in CH_3CN to yield outer sphere salts of bis(solvento) complex cations analogous to the perchlorates (vide infra). The complexes were air-stable as solids but decomposed slowly in aerobic solutions.

The solid-state structures were determined for three representative complexes, $[(L_1)Fe^{II}(NCCH_3)_2](ClO_4)_2$, $(L_6)Fe^{II}(OTf)_2$, and $[(L_8)Fe^{II}(OTf)_2]_2$ (Tables 1 and 2 and Figure 1). The first two complexes adopt the expected and essentially identical pseudooctahedral geometries characteristic of tetradentate TPA ligands, such that the unsubstituted 2-pyridylmethyl arms are arranged in a cis, rather than the more symmetric trans, configuration. This arrangement affords open cis sites opposite the amine and one unsubstituted pyridine that are filled by two exogenous ligands, either CH_3CN or triflate. The trans bite angles between opposing pyridines are significantly constrained from linearity (i.e., 151.7(1) and 151.12(7)°, respectively) by the methylene arms, but such angles to the monodentate solvent or triflate ligands are nearly linear. The coordinate bond of the monodentate ligand is significantly shorter trans to the amine than to the pyridine, by 0.051 Å for CH_3CN and 0.131 Å for triflate. However, almost all coordinate bonds in both complexes are in a narrow range of 2.18−2.22 Å, consistent with a high-spin Fe(II) state ($S = 2$).[28] One outlying bond distance (2.262 Å) is to the substituted pyridine in the L_6 complex, which is 0.06 Å longer than the corresponding bond in the L_1 complex. Because of the greater variation in coordinate bond lengths, the $(L_6)Fe^{II}(OTf)_2$ structure appears particularly unsymmetric.

(38) Connelly, N. G.; Geiger, W. E. *Chem. Rev.* **1996**, *96*, 877.
(39) Miyaura, N.; Suzuki, A. *Chem. Rev.* **1995**, *95*, 2457.
(40) Borch, R. F.; Bernstein, M. D.; Durst, H. D. *J. Am. Chem. Soc.* **1971**, *93*, 2897.
(41) Mandon, D.; Nopper, A.; Litrol, T.; Goetz, S. *Inorg. Chem.* **2001**, *40*, 4803.

Table 1. Summary of the X-ray Structure Determinations

parameter	$[(L_1)Fe^{II}(NCCH_3)_2](ClO_4)_2$	$(L_6)Fe^{II}(OTf)_2$	$[(L_8)Fe^{II}(OTf)_2]_2 \cdot CH_2Cl_2$	$[(L_1O^-)Fe^{III}(O)_{0.5}](BPh_4)$
formula	$C_{28}H_{28}N_6O_8Cl_2Fe$	$C_{27}H_{24}N_4O_7F_6O_2S_2Fe$	$C_{57}H_{54}N_8O_{12}F_{12}S_4Cl_2Fe_2$	$C_{48}H_{41}N_4O_{1.5}BFe$
formula mass (amu)	703.31	750.47	1581.92	764.51
cryst habit, size (mm)	yellow prism, 0.30 × 0.14 × 0.13	yellow slab, 0.40 × 0.13 × 0.13	colorless block, 0.21 × 0.16 × 0.05	red plate, 0.35 × 0.18 × 0.04
space group	$P2_1/n$ (monoclinic)	$P2_1/c$ (monoclinic)	$P\bar{1}$ (triclinic)	$P\bar{1}$ (triclinic)
a (Å)	10.0768(4)	12.013(2)	9.046(1)	9.8427(7)
b (Å)	11.0129(5)	9.933(2)	10.855(1)	13.9820(9)
c (Å)	28.3180(12)	25.193(2)	16.774(2)	15.508(1)
α (deg)	90	90	88.952(2)	64.763(1)
β (deg)	91.302(1)	93.057(4)	88.918(2)	77.158(1)
γ (deg)	90	90	87.495(2)	88.792(1)
V, Å^3	3141.8(2)	3001(1)	1645.0(3)	1875.6(2)
Z	4	4	1	2
D_{calc} (g cm^{-3})	1.487	1.661	1.597	1.354
GOF	1.080	1.038	1.016	1.015
R ($I > 2\sigma(I)$)	0.065	0.036	0.049	0.039
R_w	0.100	0.095	0.092	0.099

Table 2. TPA Coordinate Bonds for Iron Complexes (Bond Lengths in Å)

bond	trans donor	$[(L_1)Fe^{II}(NCCH_3)_2]^{2+}$ (tetradentate N_4, cis)	$[(L_6)Fe^{II}(OTf)_2]$ (tetradentate N_4, cis)	$[(L_8)Fe^{II}(OTf)_2]_2$ (tridentate N_3, trans)	$[(L_1O^-)_2Fe^{III}_2(O)]^{2+}$ (pentadentate N_4O)
Fe−amine		2.217(3) (N1)	2.217(2) (N4)	2.202(3) (N1)	2.210(2) (N1)
Fe−py	Phpy/py	2.193(3) (N2)	2.181(2) (N3)		2.144(2) (N2)
					2.167(2) (N3)
	$NCCH_3$	2.211(3) (N3)			
	OTf		2.215(2) (N2)		
Fe−Mepy	Mepy			2.229(3) (N2)	
				2.225(3) (N3)	
Fe−Phpy	py	2.207(3) (N4)	2.262(2) (N1)		
	oxo				2.191(2) (N4)
Fe−$NCCH_3$	py	2.159(4) (N6)			
	amine	2.108(4) (N5)			
Fe−OTf	py		2.189(2) (O61)		
	amine		2.058(2) (O51)	2.126(2) (O3A)[a]	
	OTf			2.278(2) (O1)[a]	
				2.119(2) (O4)	
Fe−oxo	Phpy				1.7897(3) (O1)
Fe−OPh	amine				1.901(1) (O2)

[a] μ_2-bridging.

The structure of $[(L_8)Fe^{II}(OTf)_2]_2$ is unique in several respects (Figure 1, Table 2). The TPA ligand was found to be tridentate, with the 6-phenyl-2-pyridylmethyl arm detached from the coordination sphere of the metal. Similar tridentate coordination was reported recently for $Fe^{III}Cl_3$ complexes of 6-substituted TPA ligands.[41] The 6-methyl substituents presumably destabilize tetradentate coordination, but this effect is difficult to gauge; even 6-Ph_3TPA can be completely bound, as in the trigonal bipyramidal complex $[LCu^{II}(NCCH_3)](ClO_4)_2$.[26] The remaining coordination sites are filled with triflates to complete a distorted octahedron, one monodentate terminal and two bidentate bridging, and form an unsupported *anti*−*anti* ditriflato-bridged dimer with an Fe(II)···Fe(II) separation of 5.774(1) Å. Although triflate bridges are observed frequently in complexes of noble metals, $[Me_3Pt^{IV}(\mu\text{-OTf})]_n$ (n = 2, 4) serving as striking examples,[42] apparently this is the initial structural report of a well-ordered triflate bridge between iron atoms in any oxidation state. The only other report is for a disordered *syn*−*syn* μ_2-triflato bridge between Fe(II) centers separated by 4.120(3) Å.[43] A *syn*−*anti* diacetato bridge with an Fe(II)−Fe(II) distance of 4.288(2) Å was reported for $[(TPA)Fe^{II}(OAc)]_2(BPh_4)_2$.[44] The ditriflato bridge obtained here is not symmetric, displaying Fe(II)−OTf bond lengths of 2.126(2) and 2.278(2) Å and respective Fe(II)−O−S angles of 155.1(2) and 129.7(1)°. Nevertheless, these parameters approach those for coordination of the terminal triflato ligand, 2.119 (2) Å and 144.9(2)°, as well as for ligation of the terminal triflates of $(L_6)Fe^{II}(OTf)_2$, 2.058(2) and 2.189(2) Å and 144.5(1) and 137.4(1)°. Direct comparison of coordinate bonds situated trans to the amine indicates the bridging triflate in the L_8 complex is displaced from the metal by 0.07 Å relative to the terminal triflate of $(L_6)Fe^{II}(OTf)_2$. Unlike the other two complexes, the 6-methyl-2-pyridylmethyl arms fold into a trans configuration, which accommodates the meridional array of triflate oxygen donor atoms. The average Fe(II)−N distance of 2.22 Å again is indicative of a high-spin configuration on the metal ion.

The various complexes of L_1−L_8 were characterized at room temperature by ^{1}H NMR spectroscopy in CD_3CN solutions as high-spin bis(solvento) complex cations of general formula $[(L)Fe^{II}(NCCD_3)_2]^{2+}$. The counteranions ($ClO_4^-$, OTf^-) were spectroscopically innocent under these conditions, as the spectra obtained from $[(L_1)Fe^{II}(NCCH_3)_2](ClO_4)_2$ and $(L_1)Fe^{II}(OTf)_2$ were identical except for the resonance of free CH_3CN.

Observed pyridyl resonances (Table S2) were broad, ca. 40−250 Hz, and subject to large isotropic shifts over a ca. −10 to

(42) Schlecht, S.; Magull, J.; Fenske, D.; Dehnicke, K. *Angew. Chem., Int. Ed. Engl.* **1997**, *36*, 1994.
(43) (a) Herold, S.; Pence, L. E.; Lippard, S. J. *J. Am. Chem. Soc.* **1995**, *117*, 6134. (b) Herold, S.; Lippard, S. J. *J. Am. Chem. Soc.* **1997**, *119*, 145.
(44) Ménage, S.; Zang, Y.; Hendrich, M. P.; Que, L., Jr. *J. Am. Chem. Soc.* **1992**, *114*, 7786.

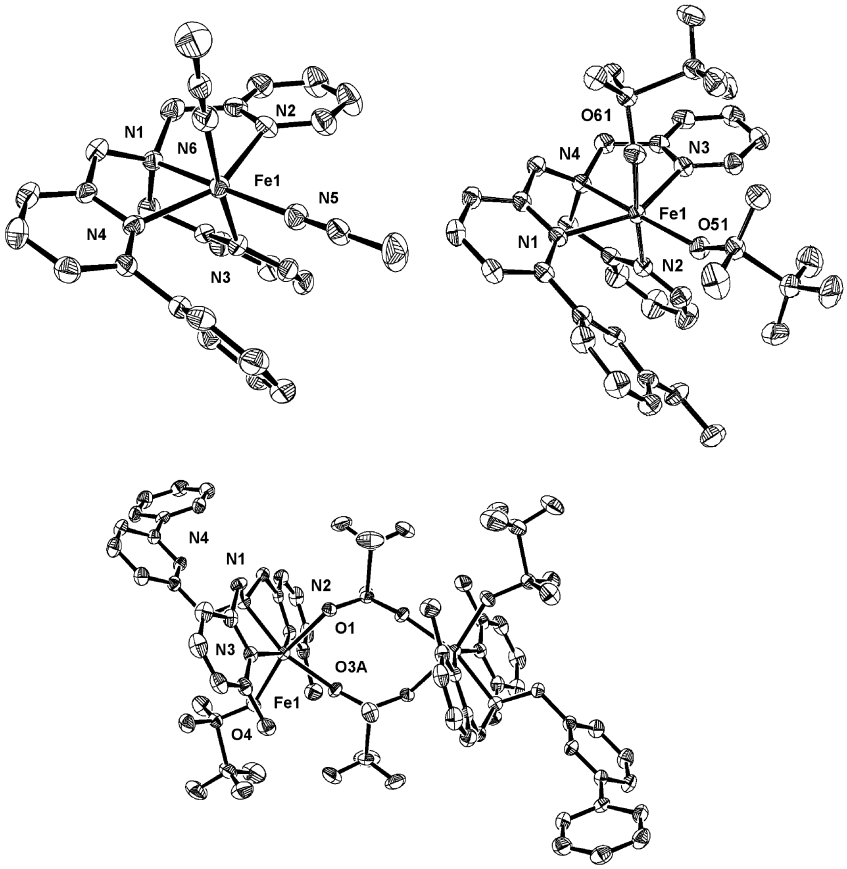

Figure 1. ORTEP diagrams of the complex cation of $[(L_1)Fe^{II}(NCCH_3)_2]^{2+}$ (top left) and the $(L_6)Fe^{II}(OTf)_2$ (top right) and $[(L_8)Fe^{II}(OTf)_2]_2$ (bottom) complexes (ellipsoids drawn at 50% level; hydrogen atoms omitted for clarity).

106 ppm range, indicating that the paramagnetic $S = 2$ spin state was retained for Fe(II) in solution (Figure 2). The 2-pyridylmethyl signals were analogous to those reported for $[(6\text{-MeTPA})Fe^{II}(NCCD_3)]^{2+}$,[28] as no systematic trends in chemical shifts were induced by arene substitution. The paramagnetic contact shifts are governed primarily by σ-spin delocalization effects,[45] so that the shifts of ligand resonances increase with proximity to the metal ion: α, $NCH_2Py > \beta, \beta' > \gamma, \gamma'$. There was no basis to distinguish the α-pyridyl and methylene resonances. Assignments of the sharper β, β' and γ, γ' resonances were obvious from a 2:1 intensity pattern and cross-peaks were detected by the COSY technique for L_1. Appearance of a 2:1 pattern was consistent with effective mirror plane symmetry bisecting the unsubstituted pyridines and along the phenyl-substituted arms; thus, refolding of the unsymmetric ligand field evident in the solid state must be dynamic on the NMR time scale.

Three resonances observed near the diamagnetic region of the $(L_1)Fe^{II}(NCCD_3)_2]^{2+}$ spectrum in a 2:1:2 intensity ratio at 2.3, 0.1, -0.8 ppm were assigned to the *meta*, *para*, and *ortho* protons of the phenyl ring, respectively, as the latter was broadened by the proximal paramagnet. These signals were absent in the spectrum of the d_5-Ph isotopomer (Figure 2B). Substitution at the *meta* position breaks the ring symmetry, so that four phenyl resonances of equal intensity were observed for complexes of L_2-L_6. Similarly, two equally intense resonances in the diamagnetic region observed for the L_7 complex cation were assigned to the *ortho* and *meta* protons.

The dimeric $[(L_8)Fe^{II}(OTf)_2]_2$ complex dissolved in CH_3CN to yield an analogous $[(L_8)Fe^{II}(NCCD_3)_2]^{2+}$ complex and free triflate counteranions, as observed by NMR spectroscopy (Figure 2C). The ^1H NMR spectrum was comparable to that of the L_1 complexes, except paramagnetically shifted signals were more widely dispersed, and the downfield α pyridyl proton resonance was replaced by an intense methyl signal shifted upfield to -29.1 ppm by spin polarization.[45] The phenyl ring protons were essentially unshifted, appearing at 7.7 (*meta*), 7.3 (*ortho*), and 6.9 (*para*) ppm, and the *ortho* resonance was broadened significantly. The ^{19}F spectrum consisted of a single, sharp ($\Delta\nu_{1/2} = 80$ Hz) resonance at -72.2 ppm. The complex yielded quite different spectra when dissolved in CD_2Cl_2, however. The ^1H spectrum consisted largely of several poorly resolved signals in the diamagnetic region, displaying only three broad, paramagnetically shifted resonances in a 1.0:1.0:1.5 intensity ratio at 51.7, 43, and -23 ppm. A single broad ($\Delta\nu_{1/2} = 900$ Hz) peak was observed in the ^{19}F spectrum at -47.9 ppm. These data are most consistent with a structure like that determined by X-ray crystallography, which retains bound triflates and two coordinated 6-methyl-2-pyridylmethyl arms giving paramagnetically shifted and unresolved β, methylene, and methyl resonances, as well as an uncoordinated 6-phenyl-2-pyridylmethyl arm. In contrast, ^1H NMR spectra of $(L_1)Fe^{II}(OTf)_2$ in CD_3CN and CD_2Cl_2 were quite similar, exhibiting a slightly

(45) Ming, L.-J. In *Physical Methods in Bioinorganic Chemistry*; Que, L., Jr., Ed.; University Science Books: Sausalito, CA, 2000; Chapter 8.

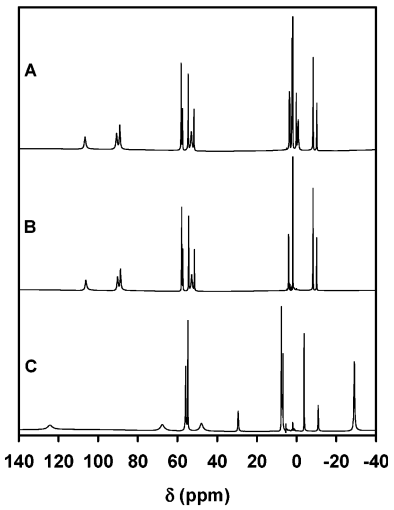

Figure 2. ^{1}H NMR spectra (500 MHz) of the following: $[(L_1)Fe^{II}(NCCH_3)_2](ClO_4)_2$ (A); $[(d_5\text{-}L_1)Fe^{II}(NCCH_3)_2](ClO_4)_2$ (B); $[(L_8)Fe^{II}(OTf)_2]_2$ (C) recorded at 293 K as CD_3CN solutions.

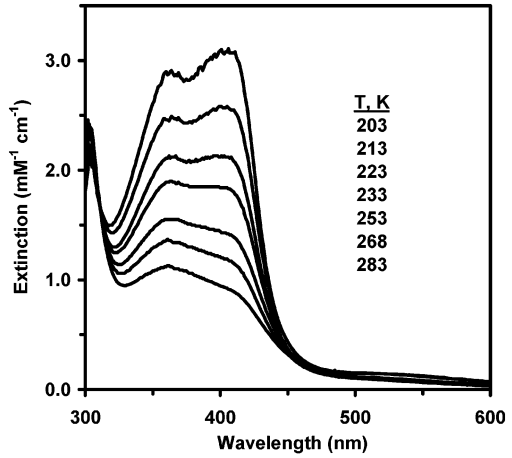

Figure 3. Temperature-dependent UV−visible spectra of $[(L_1)Fe^{II}(NCEt)_2]^{2+}$ in EtCN solution.

wider paramagnetic shift range in the latter solvent. Analogous results were obtained in CD_2Cl_2 for $(L_n)Fe(OTf)_2$ ($n = 2-7$).

Solutions of the neutral triflate complexes of L_1-L_7 in CH_2Cl_2 were invariably pale yellow, and the UV−visible spectra accordingly were nearly featureless, consisting only of a slight shoulder ($\lambda_{max} = 350-380$ nm, $\epsilon_{max} = 500-800$ M^{-1} cm^{-1}) on the tail of intense pyridine $\pi-\pi^*$ bands in the UV region. The same was true of $[(L_8)Fe^{II}(OTf)_2]_2$ dissolved either in CH_2Cl_2 or CH_3CN. In contrast, UV−visible spectra recorded from organonitrile solutions of $[(L_n)Fe^{II}(NCCH_3)_2]^{2+}$ ($n = 1-7$) contained strong features at 360 ± 5 and 400 ± 5 nm presumably assignable to iron(II)-to-pyridine MLCT bands, as well as a broad weak ligand field band at 550 nm (Figure 3). The extinctions of these bands were found to be strongly temperature-dependent, as illustrated for a propionitrile (EtCN) solution of $[(L_1)Fe^{II}(NCCH_3)_2](ClO_4)_2$ (Figure 3). This absorption imparted distinct color to solutions even at room temperature, and cooling of propionitrile solutions below ca. 210 K resulted in a reversible color change to brick red.

The color change is consistent with well-known spin crossover of d^6 Fe(II) complexes between $S = 2$ and $S = 0$ spin states.[46,47] The failure to observe color changes in CH_2Cl_2 solutions of the triflato complexes, and for the 6-methyl

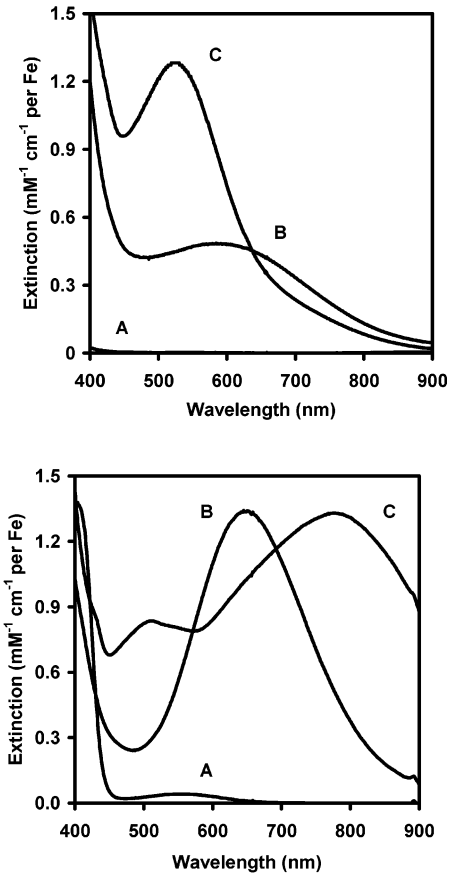

Figure 4. Visible spectra of CH_3CN solutions of $[(L)Fe^{II}(NCCH_3)_2]^{2+}$ (A), $[(L)Fe^{III}(OO^tBu)]^{2+}$ intermediate (B), and $[(LO^-)Fe^{III}]^{2+}$ product (C), for L_1 recorded at 228 K (bottom) and L_8 recorded at 293 K (top).

substituted (L_8) complex cation even in organonitrile solution, is consistent with the weaker ligand fields afforded to the metal ion. Similar behavior was observed by ^{1}H NMR spectroscopy for closely related complexes. $[(TPA)Fe^{II}(OTf)_2]$ exhibited paramagnetically shifted resonances in CD_2Cl_2 but not in CD_3CN due to formation of the low-spin $[(TPA)Fe^{II}(NCCH_3)_2]^{2+}$;[28,46] however, increasing paramagnetic shifts were observed for the latter at elevated temperatures (e.g., $\delta(\alpha\text{-py}) = 60$ ppm at 353 K).[46] X-ray crystallography also indicated a low-spin solid-state structure for $[(TPA)Fe^{II}(NCCH_3)_2](ClO_4)_2$ and a high-spin configuration for $[(6\text{-}Me_3TPA)Fe^{II}(NCCH_3)_2](ClO_4)_2$, based on Fe−N bond lengths.[28] Unfortunately, the putative spin crossover of $[(L_1)Fe^{II}(NCCD_3)_2]^{2+}$ was not conveniently observable by ^{1}H NMR spectroscopy near the freezing point of CD_3CN (ca. 230 K).

Reaction with ^{t}BuOOH. UV−visible spectroscopy is a convenient method to monitor reactions of the complexes with ^{t}BuOOH in CH_3CN (Figure 4). Addition of the peroxide ($[^t\text{BuOOH}]_0 \leq 3.5$ mM) to 1.0 mM solutions of the complexes prompted eventual development of stable and intense visible chromophores (e.g., spectrum C in Figure 4 bottom, $\lambda_{max} = 780$ nm for L_1). The L_2-L_5 complexes also reacted to form similar chromophores, which were blue-shifted relative to the L_1 product for L_2-L_4 by the presence of electron-withdrawing aryl substituents and red-shifted for L_5. The product solutions of the

(46) Diebold, A.; Hagen, K. S. *Inorg. Chem.* **1998**, *37*, 215.
(47) (a) Gütlich, P. *Struct. Bonding* **1981**, *44*, 83. (b) Toftlund, H. *Coord. Chem. Rev.* **1989**, *94*, 67. (c) Gütlich, P.; Garcia, Y.; Goodwin, H. A. *Chem. Soc. Rev.* **2000**, *29*, 419.

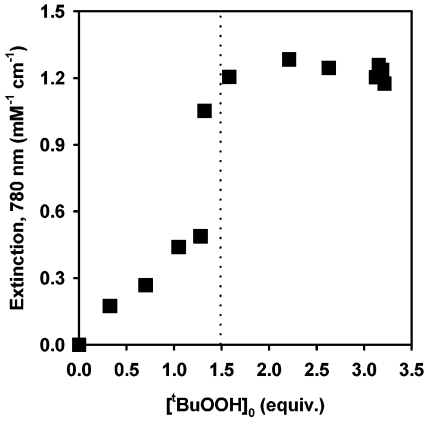

Figure 5. Spectrophotometric yields of the blue $[(L_1O^-)Fe^{III}(NCCH_3)]^{2+}$ species, observed at 780 nm, as a function of added equivalents of ^{t}BuOOH to $[(L_1)Fe^{II}(NCCH_3)_2](ClO_4)_2$ (1.05 ± 0.07 mM) in CH_3CN at 228 K.

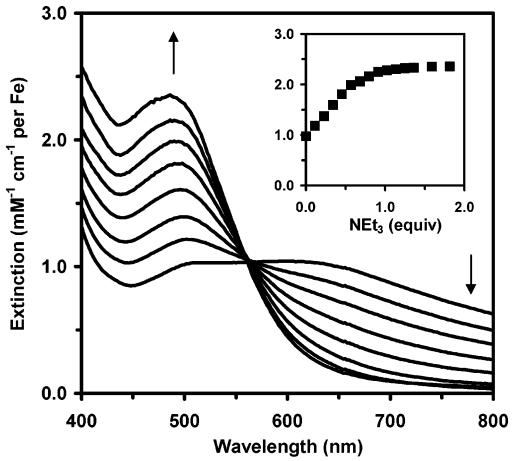

Figure 6. Spectrophotometric titration of the violet $[(L_1O^-)Fe^{III}(OH_2)]^{2+}$ species with triethylamine to afford orange $[(L_1O^-)_2Fe^{III}_2(\mu\text{-}O)]^{2+}$ at 293 K.

most electron-rich arenes (i.e., L_6, L_7) bleached to give an uncharacterized yellow solution, presumably due to overoxidation. Partial bleaching of the other products was problematic only at higher peroxide stoichiometries and warmer temperatures. The properties of these visible chromophores are consistent with their assignment to phenolate-to-iron(III) LMCT bands afforded by *ortho*-hydroxylation of the pendant arenes. For complexes of L_1−L_7, the reactions were complete within seconds at room temperature, or after several hours at 228 K, and were not affected by the presence of dioxygen. $[(L_8)Fe^{II}(NCCH_3)_2]^{2+}$ reacted slowly with 3.5 mM ^{t}BuOOH at room temperature, and a stable magenta chromophore (spectrum C in Figure 4 top, $\lambda_{max} = 525$ nm) was obtained after several hours.

Addition of variable quantities of ^{t}BuOOH to solutions of $[(L_1)Fe^{II}(NCCH_3)_2]^{2+}$ (average concentration = 1.05 ± 0.07 mM) under N_2 at 228 K established that a minimum peroxide to complex stoichiometry of 1.5:1.0 was necessary and sufficient to obtain the maximum spectrophotometric yield (Figure 5). Further additions of peroxide in modest excess did not affect the yield. Product solutions exhibited a color change to violet ($\lambda_{max} = 600$ nm) in the presence of excess water (ca. 10 mM) at 293 K, and titration of such a solution with 0.9 ± 0.2 equiv of NEt_3 prompted a further color change to orange ($\lambda_{max} = 486$ nm) (Figure 6). Crystals of the orange product obtained by metathesis with $NaBPh_4$ were redissolved in CH_3CN at room

Scheme 4

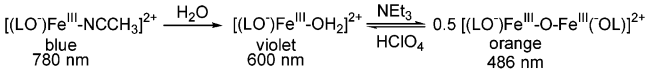

temperature to determine that the maximum spectrophotometric yield corresponds to 87% phenolate formation ($\epsilon_{max} = 2650$ M^{-1} cm^{-1}/iron at 298 K).

A mass spectrum of the blue L_1 product solution, obtained by electrospray ionization, contained two parent cations at *m*/*z* 536 and 939, whose masses and observed isotope distributions were consistent with their respective formulation as $[(L_1O^-)Fe^{III}(ClO_4)]^+$ and $\{[(L_1O^-)_2Fe^{III}_2(O)](ClO_4)\}^+$. The orange solutions obtained by NEt_3 addition gave only the latter ion, and a cation with *m*/*z* 1209 was observed from a solution of the isolated tetraphenylborate salt, consistent with the formulation $[(L_1O^-)_2Fe^{III}_2(O)](BPh_4)]^+$. The L_8 product solution yielded parent ions at *m*/*z* 614 and 1095 corresponding to $[(L_8O^-)Fe^{III}(OTf)]^+$ and $[(L_8O^-)_2Fe^{III}_2(O)](OTf)]^+$, respectively.

The mass spectral and UV−visible data suggest that the immediate products of L_1 and L_8 complex oxidation are $[(L_1O^-)Fe^{III}(X)]^{2+}$ and $[(L_8O^-)_2Fe^{III}_2(O)]^{2+}$, respectively. The progressive blue shift of the visible absorption maximum for $[(L_1O^-)Fe^{III}(X)]^{n+}$ reflects equilibria at the sixth ligand site (Scheme 4), presumably displacement of CH_3CN with more basic aqua and oxide ligands, which diminish the Lewis acidity of the iron(III) center.[48] Similarly, spontaneous formation of the $(L_8O^-)Fe^{III}$ oxo-bridged dimer in solution and the red shift of its chromophore compared to that of the orange L_1 product are consistent with the decreased basicity of the 6,6-dimethyl-substituted ligand.

Examination of the orange L_1 product complex by X-ray crystallography confirmed an oxo-bridged dimeric structure of crystallographically equivalent iron(III) complexes of modified N_4O-pentadentate ligands, $[(L_1O^-)_2Fe^{III}_2(\mu\text{-}O)](BPh_4)_2$ (Tables 1 and 2 and Figure 7). The oxo bridge is symmetrically constrained to linearity. The phenolate oxygen is situated trans to the amine, so that these form a meridional donor array along with the substituted pyridine. This rigid arrangement must develop during the hydroxylation reaction, which suggests a specific geometry for reactive intermediates (vide infra). The *ipso* torsional angle of 28(1)° accommodates an Fe^{III}−O bond length of 1.901(1) Å and a nearly linear O2−Fe1−N1 angle of 165.45(6)°. The unsubstituted 2-pyridylmethyl arms fold into a trans arrangement on either side of the phenolate, as opposed to the cis arrangement found for $[(L_1)Fe^{II}(NCCH_3)_2]^{2+}$. An average pyridine coordinate bond length of 2.18 Å indicates a high-spin ($S = 5/2$) state for the iron(III) ions.[28]

The ^{1}H NMR spectrum of $[(L_1O^-)_2Fe^{III}_2(\mu\text{-}O)](BPh_4)_2$ in CD_3CN solution consisted of broad (ca. 100 Hz) signals distributed over a narrow chemical shift range (−2 to 30 ppm), indicative of the expected strong antiferromagnetic coupling of the $S = 5/2$ metal ions through the oxo bridge (Figure S1).[49] Given ideal C_{2h} symmetry, the 42 protons of the dimeric complex cation will give rise to 14 total resonances, 7 each with 2H and 4H intensities. Eight signals corresponding to 32

(48) (a) Pyrz, J. W.; Roe, A. L.; Stern, L. J.; Que, L., Jr. *J. Am. Chem. Soc.* **1985**, *107*, 614. (b) Que, L., Jr. In *Biological Applications of Raman Spectroscopy*; Spiro, T. G., Ed.; John Wiley & Sons: New York, 1988; Vol. 3, pp 491−521.

(49) (a) Wu, F.-J.; Kurtz, D. M., Jr. *J. Am. Chem. Soc.* **1989**, *111*, 6563. (b) Norman, R. E.; Yan, S.; Que, L., Jr.; Backes, G.; Ling, J.; Sanders-Loehr, J.; Zhang, J. H.; O'Connor, C. J. *J. Am. Chem. Soc.* **1990**, *112*, 1554.

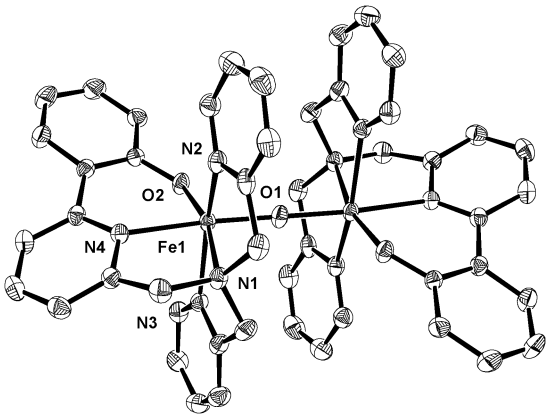

Figure 7. ORTEP diagram of the complex cation $[(L_1O^-)_2Fe^{III}_2(\mu\text{-}O)]^{2+}$ (ellipsoids drawn at 50% level; hydrogen atoms omitted for clarity).

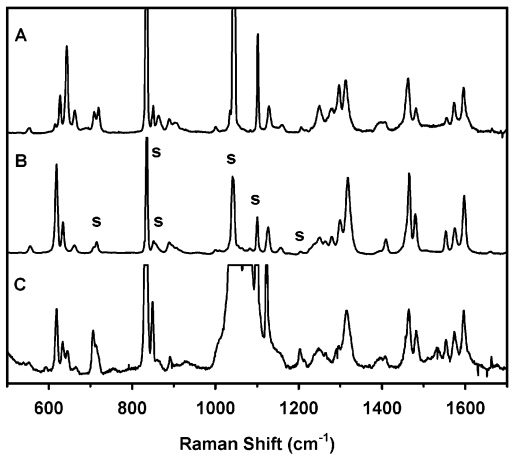

Figure 8. Resonance Raman spectra of blue $[(L_1O^-)Fe^{III}(NCCH_3)]^{2+}$ (A, 632.8 nm excitation), orange $[(L_1O^-)_2Fe^{III}_2(O)]^{2+}$ (B, 514.5 nm excitation), and magenta $[(L_8O^-)_2Fe^{III}_2(O)]^{2+}$ (C, 514.5 nm excitation) chromophores in frozen CD_3CN solutions. Solvent features are denoted (s). See Table S3 for a listing of frequencies.

protons were observed at 31 (8H), 16.9 (8H), 15.8 (4H), 15.2 (2H), 12.5 (2H), 11.5 (2H), 9.4 (2H), and −1.9 ppm (4H). Integration indicated the signals of eight more protons were coincident with resonances of the BPh_4^- counterions. The remaining two protons were not accounted for but could have been coincident with the residual solvent resonance. Thus, the observed NMR spectrum was consistent with the dimeric structure determined by X-ray crystallography.

The blue $[(L_1O^-)Fe^{III}(X)]^{2+}$ product was further characterized by resonance Raman spectroscopy of frozen acetonitrile solutions using 632.8 nm laser excitation into the LMCT band (Figure 8A). The typical response of *para*-substituted phenolates (e.g., tyrosinate) coordinated to iron(III) consists of four bands corresponding to aromatic deformations near 1170, 1270, and 1500 and 1600 cm^{-1}, respectively, as well as a band near 600 cm^{-1} assigned to the $\nu(Fe^{III}-OAr)$ mode.[48] These modes split into groups of additional bands for phenolates with lower symmetry, especially for those with *ortho*-imine substituents (e.g., salen complexes).[50] In so far as the L_1 phenolate complex is similar, the present results can be interpreted analogously (Table S3). Notably, there is an intense band at 644 cm^{-1} that can be assigned to the $\nu(Fe^{III}-OAr)$ mode.

The orange dinuclear $[(L_1O^-)_2Fe^{III}_2(\mu\text{-}O)]^{2+}$ complex was also characterized by resonance Raman spectroscopy, using 514.5 nm laser excitation of a frozen CD_3CN solution (Figure 8B). Several resonance-enhanced phenolate modes were observed in the 600−1600 cm^{-1} region, but the spectrum was distinct from that of the mononuclear blue species. In particular, the $\nu(Fe^{III}-OAr)$ peak downshifted to 619 cm^{-1}, consistent with the weakening of the iron(III)−phenolate interaction in the presence of an oxo bridge. Consistent with its formulation as $[(L_8O^-)_2Fe^{III}_2(\mu\text{-}O)]^{2+}$, a spectrum of the L_8 product solution was very similar to that of $[(L_1O^-)_2Fe^{II}_2(\mu\text{-}O)]^{2+}$ (Figure 8C).

Because of the stability of the phenolate chromophores for L_1-L_5 and L_8, the complexes could be disrupted by acid treatment, and the free ligands could be recovered by extraction into $CDCl_3$ with a typical efficiency of 60−70%. ^1H NMR spectroscopy indicated that the extract solutions were mixtures of *o*-hydroxylated (50−90%) ligands and residual unmodified precursors (Table 3). No products were observed that would indicate competing oxidative pathways, such as 2-pyridinecarboxaldehydes afforded by N-dealkylation of the tertiary amine.[51] The ^1H NMR spectrum of recovered L_1 product matched exactly that of a sample of L_1OH prepared by an independent route; resonances assigned to the phenol ring were absent in the d_5-L_1 product spectrum.

Fractional yields of *ortho*-hydroxylated ligands obtained from consistent 3.5:1.0 ^{t}BuOOH−complex stoichiometries were not strongly perturbed by the nature of the *meta* substituent. However, two product isomers are possible for L_2-L_5, with hydroxylation occurring at either *ortho* carbon, *ortho* or *para* to the substituent. Only the *para*-nitrophenol isomer was observed for L_2OH (Figure 9). In contrast, L_3 (*m*-CF_3) and L_4 (*m*-Cl) yielded both isomers, with the *ortho* rotamer slightly favored. This was confirmed in the former case by ^{19}F NMR spectroscopy, which revealed two product resonances (−61.8, −63.4 ppm) near the resonance of the starting ligand (−63.0 ppm), all of approximately equal intensity. The spectrum of L_5 product was consistent with phenol formation but was sufficiently convoluted to prevent assignment of specific isomers. The L_6 and L_7 phenolate complexes apparently were susceptible to overoxidation, and no organic products were isolated by extraction. The phenol resonances of the L_8 product were essentially identical to those observed for L_1.

The NMR product solutions for L_1-L_5 were characterized in parallel by mass spectrometry (Table S4). In each case, two parent peaks were observed at masses calculated for protonated monocations of the phenyl and phenol species and with the expected isotopomeric distributions. Consistent with oxygen atom addition, the parent ions were separated by 16 amu, appearing at *m*/*z* 367 and 383 for L_1H^+ and $L_1OH_2^+$ ions, respectively. Moreover, d_5-L_1 derived ions at *m*/*z* 372 and 387, the 15 amu difference demonstrating that oxygen atom addition was coupled to C−D bond labilization.

Spectroscopic Detection of Reaction Intermediates. The hydroxylation reactions of the L_1-L_7 complexes were extremely rapid at room temperature, requiring only seconds for the stable phenolate chromophores to develop at millimolar concentrations. However, at 258 K monotonic development of the phenolate-to-iron(III) LMCT chromophore was observed over a ca. 20-m

(50) Carrano, C. J.; Carrano, M. W.; Sharma, K.; Backes, G.; Sanders-Loehr, J. *Inorg. Chem.* **1990**, *29*, 1865.

(51) Mahapatra, S.; Halfen, J. A.; Tolman, W. B. *J. Am. Chem. Soc.* **1996**, *118*, 11575.

Table 3. ^{1}H NMR Data for Extracted Phenols ($CDCl_3$ Solutions, δ in ppm, J_{HH} in Hz)

		ortho isomer				*para* isomer			
phenol	*meta*-X	H_o	H_m	H_p	mole fraction[a]	H_o	H_p	H_m	mole fraction[a]
L_1OH	H	7.76	6.91 (ddd; 7.4, 1.5)	7.32 (ddd; 7.1, 1.5)	*b*	*b*	*b*	7.05 (dd; 8.3)	0.85
L_2OH	NO_2				0.00	8.75 (d; 2.5)	8.21 (dd; 9.0, 3.0)	7.10 (d; 9.5)	0.62
L_3OH	CF_3	7.95 (d; 7.0)	6.94 (dd; 7.7)	7.60	0.39	8.03 (s)	7.54	7.11 (d; 8.5)	0.32
L_4OH	Cl	7.66 (8.0)	6.86 (dd; 8.0)	7.42	0.48		7.27	6.99 (d; 8.5)	0.35
L_8OH	H	7.78 (dd)	6.89 (ddd; 8.5, 1.2)	7.30 (ddd; 6.8, 1.7)	*b*	*b*	*b*	7.03 (dd; 8.5)	0.46

[a] Fraction of total extracts; balance is unreacted ligand. [b] Degenerate.

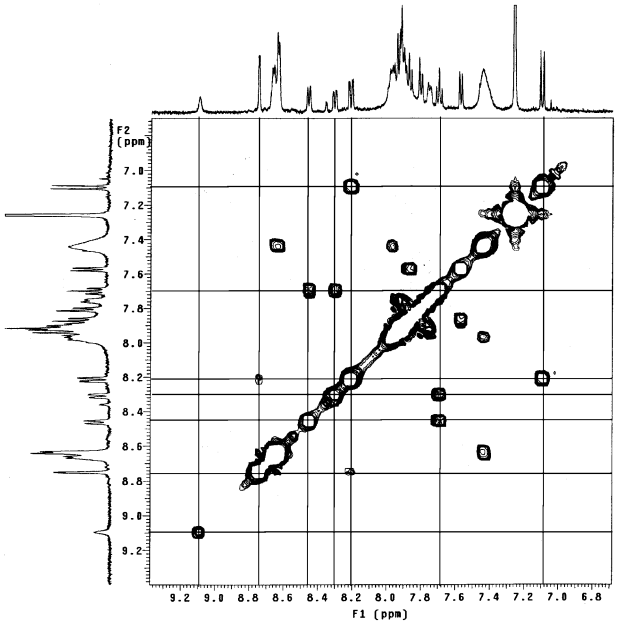

Figure 9. ^{1}H COSY NMR spectrum of extracts from reaction of ^{t}BuOOH and $[(L_2)Fe^{II}(NCCH_3)_2]^{2+}$ in $CDCl_3$ solution. Cross-peaks are indicated for phenyl resonances of L_2 and phenol resonances of L_2OH. Only one phenol isomer is apparent.

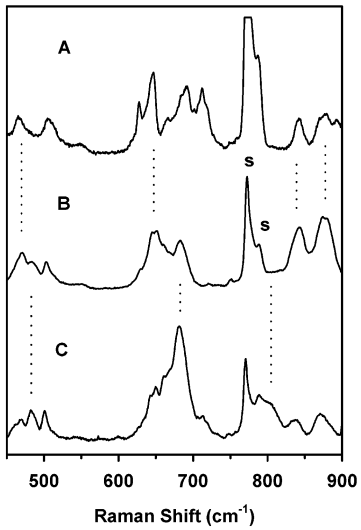

Figure 10. Resonance Raman spectra of $[(L)Fe^{III}(OO^tBu)]^{2+}$ peroxo intermediates recorded from frozen CH_3CN solutions for L_8 (A, 632.8 nm excitation) and L_1 (B, 568.2 nm excitation, and C, 632.8 nm excitation). Dotted lines denote features corresponding to high-spin (A and B) and low-spin (B and C) isomers. Solvent features are denoted (s).

interval for the reaction of $[(L_1)Fe^{II}(NCCH_3)_2]^{2+}$ (1.0 mM) and ^{t}BuOOH (3.0 mM). The same reaction required several hours to reach completion below 233 K, and a transient intermediate was detected prior to accumulation of the phenolate chromophore (B in Figure 4, bottom). A strong visible chromophore ($\lambda_{max} = 650$ nm, $\epsilon_{max} = 1300$ M^{-1} cm^{-1}) developed over several minutes, and this was not affected by the *meta* arene substitution pattern, which indicated that phenolate complexes had yet to develop.

Further spectroscopic studies led to the assignment of the intermediate chromophore as $Fe^{III}-OOR$ LMCT.[28,52] Resonance Raman spectra recorded from a reaction solution of $[(L_1)Fe^{II}(NCCH_3)_2]^{2+}$ and ^{t}BuOOH frozen at the time of maximum intermediate extinction revealed resonance-enhanced vibrations characteristic of iron(III)−alkylperoxo complexes (Figure 10 B,C and Table 4). From comparison with spectra of low-spin $[(TPA)Fe^{III}(OO^tBu)]^{2+}$,[21d,28] high-spin $[(6\text{-}Me_3TPA)Fe^{III}(OO^tBu)]^{2+}$,[28] and related complexes,[53] it can be deduced that the complexity of the observed spectrum reflects a mixture of both high- and low-spin isomers of $[(L_1)Fe^{III}(OO^tBu)]^{2+}$. The presence of two distinct alkylperoxo species was clearly indicated by different degrees of resonance enhancement at various excitation wavelengths, with longer wavelengths favoring enhancement of features of the low-spin isomer. The red shift of the absorption maximum for the low-spin isomer relative to that for the high-spin isomer is also consistent with results obtained for the TPA series.[28] The presence of spin isomers was supported by an EPR spectrum of the mixture, which consists of a signal at $g = 8.4$, corresponding to a high-spin $S = 5/2$ iron(III) ion, and signals at $g = 2.18$, 2.11, and 1.97 assignable to a low-spin $S = 1/2$ iron(III) ion. (Table 4). The 6-PhTPA ligand is thus analogous to 6-MeTPA in supporting a spin-isomeric mixture of iron(III) peroxo complexes.[28]

As for the iron(II) complex precursors, spin isomerism in the $[(L_1)Fe^{III}(OO^tBu)]^{2+}$ intermediate was greatly affected by solvent. Treatment of $[L_1Fe(OTf)_2]$ with excess ^{t}BuOOH at 233 K in CH_2Cl_2 resulted in the immediate formation of a purple chromophore ($\lambda_{max} = 566$ nm, Figure S2), which was significantly blue-shifted compared to that of the intermediate obtained in CH_3CN. A resonance Raman spectrum of this chromophore contained features typical of a high-spin iron(III) alkylperoxo species only (Figure S3), and the absence of a low-spin isomer was confirmed by EPR spectroscopy, Table 4. Nevertheless, the purple species in CH_2Cl_2 decomposed on a time scale comparable to the same reaction in CH_3CN to produce a stable blue chromophore ($\lambda_{max} = 600$ nm, Figure S2). The resonance Raman spectrum of this product was consistent with assignment to an iron(III) phenolate monomer, $\nu(Fe^{III}-OAr) = 644$ cm^{-1} (Figure S4 and Table S3).

(52) (a) Lehnert, N.; Ho, R. Y. N.; Que, L., Jr.; Solomon, E. I. *J. Am. Chem. Soc*. **2001**, *123*, 8271. (b) Lehnert, N.; Ho, R. Y. N.; Que, L., Jr.; Solomon, E. I. *J. Am. Chem. Soc*. **2001**, *123*, 12802.

(53) (a) Ménage, S.; Wilkinson, E. C.; Que, L., Jr.; Fontecave, M. *Angew. Chem., Int. Ed. Engl*. **1995**, *34*, 203. (b) Wada, A.; Ogo, S.; Watanabe, Y.; Mukai, M.; Kitagawa, T.; Jitsukawa, K.; Masuda, H.; Einaga, H. *Inorg. Chem*. **1999**, *38*, 3592. (c) Ogihara, T.; Hikichi, S.; Akita, M.; Uchida, T.; Kitagawa, T.; Moro-oka, Y. *Inorg. Chim. Acta* **2000**, *297*, 162.

Table 4. Spectroscopic Data for (*tert*-Butylperoxo)iron(III) Complexes

complex	solvent	spin state	UV–vis (nm)	EPR (*g*-values)	resonance Raman (cm^{-1})				ref
$[(TPA)Fe(OO^tBu)]^{2+}$	MeCN	low	600	2.19, 2.14, 1.98	490	696	796		28
$[(TPA)Fe(HOBz)(OO^tBu)]^{2+}$	MeCN	low	598	2.19, 2.12, 1.97	490	696	796		21d
$[(6\text{-}MeTPA)Fe(OO^tBu)]^{2+}$	MeCN	low	598	2.20, 2.12, 1.97	488	682	790		28
	MeCN	high		4.3	469	648	842	878	
$[(L_1)Fe(OO^tBu)]^{2+}$	MeCN	low	650	2.18, 2.11, 1.98	484	682	808		*a*
	MeCN	high		8.4, 4.3	471	650	842	878	
$[(L_1)Fe(OO^tBu)]^{2+}$	CH_2Cl_2	high	566	8.6, 4.3	469	644	840	873	*a*
$[(L_8)Fe(OO^tBu)]^{2+}$	MeCN	high	590	7.6, 4.3	467	647	842	876	*a*
$[(6\text{-}Me_3TPA)Fe(OO^tBu)]^{2+}$	MeCN	high	562	4.3	468	637	842	877	28
$[(6\text{-}Me_3TPA)Fe(O_2CPh)(OO^tBu)]^{+}$	CH_2Cl_2	high	510	4.3	463	646	844	885	63
$[(BPPA)Fe(OO^tBu)]^{2+}$	MeCN	high	613	7.58, 5.81, 4.25, 1.82	469	629	838	873	53b
$[Tp^{tBu,iPr}Fe(OO^tBu)]^{+}$	Et_2O	high	501	9.9, 4.3		606		892	53c
$[(bpy)_2Fe(HOBz)(OO^tBu)]^{2+}$	MeCN	low	640	2.18, 2.12, 1.98		678	808		53a

[a] This work.

Substitution of α-methyl substituents for hydrogen to afford $[(L_8)Fe^{II}(NCCH_3)_2]^{2+}$ affected the chemistry greatly. The reaction with ^{t}BuOOH (3.5 equiv) required several hours to reach completion even at 293 K; nevertheless an $Fe^{III}-OO^tBu$ intermediate was observed readily (λ_{max} = 590 nm, B in Figure 4, top) prior to formation of the phenolate product. Examination of the peroxo intermediate by resonance Raman and EPR methods indicated the presence of a single, high-spin isomer (Table 4 and Figure 10A). The α-methyl substituents clearly prevent accumulation of the low-spin isomer, as reported for 6-Me_3TPA,[25] and dramatically slow the conversion of the iron(III) alkylperoxo intermediate to the $[(L_8O^-)_2Fe^{III}_2(O)]^{2+}$ product.

Mechanistic Probes. Additional mechanistic insights into the arene hydroxylation were sought from a number of experiments involving either isotope labels or reactive intermediates. The former category included transfers of ^{18}O label from peroxide to the phenolate, as well as retention and migration of ^2H label on the arene. The latter involved reactive trapping of alkoxy radicals (RO•).

The origin of the phenolate oxygen was determined from ^{18}O isotope labeling studies. Thus, reaction of $[L_1Fe^{II}(NCCH_3)_2]^{2+}$ with *tert*-butyl hydroperoxide fully enriched with ^{18}O at the terminal oxygen (i.e., $^tBu^{16}O^{18}OH$)[25] resulted in formation of completely enriched phenoxide complex, as demonstrated in parallel by mass spectrometry and resonance Raman spectroscopy. An electrospray mass spectrum of the product dimer isolated as the bis(tetraphenylborate) salt revealed a single parent ion at *m*/*z* 1213, its mass and isotope distribution pattern being fully consistent with its formulation as $\{[(L_1{}^{18}O^-)_2Fe^{III}_2(\mu\text{-}O)](BPh_4)\}^+$. The lack of significant intensity at *m*/*z* 1209 indicated full retention of the oxygen isotope label. Furthermore a resonance Raman spectrum of the isotopomeric dimer revealed a ca. 8 cm^{-1} downshift of the ν(Fe-^{18}OAr) Raman mode from 619 cm^{-1} observed at normal isotope abundance (Figure 11A) to 611 cm^{-1} (Figure 11D). These data are uniquely consistent with derivation of the phenolate oxygen from the terminal oxygen atom of ^{t}BuOOH.

Reactions were also carried out in the presence of H_2O isotopomers to determine whether solvent incorporation into the oxidation product might occur. Indeed, partial ^{18}O enrichment of the resulting phenolate ligand was obtained from reaction of $[L_1Fe^{II}(NCCH_3)_2]^{2+}$ with the normal ^{t}BuOOH isotopomer in the presence of $H_2{}^{18}O$ (20 vol %), as indicated by the appearance

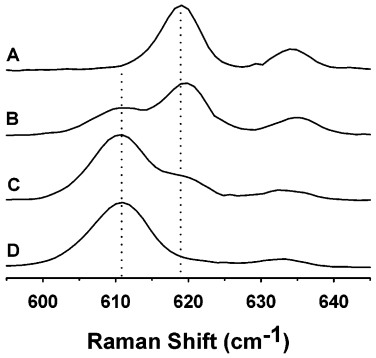

Figure 11. Detail of resonance Raman spectra of $[(L_1O^-)_2Fe^{III}_2(O)]^{2+}$, illustrating effects of ^{18}O isotope incorporation on the $\nu(Fe^{III}-OPh)$ band. Samples were prepared with normal ^{t}BuOOH (A), normal ^{t}BuOOH and 20 vol % $H_2{}^{18}O$ (B), $^tBuO^{18}OH$ and 20 vol % normal H_2O (C), and $^tBuO^{18}OH$ (D). Spectra were obtained from samples in frozen acetonitrile using 514.5 nm laser excitation.

of a feature attributed to $\nu(Fe-{}^{18}OAr)$ (Figure 11B). Conversely, partial depletion of label was observed from the reaction with $^tBuO^{18}OH$ in the presence of excess $H_2{}^{16}O$ (Figure 11C). These results indicate that the hydroxylation mechanism must involve an oxidizing species that is capable of exchange with exogenous water.[27,54]

Enzymatic arene hydroxylations are often associated with 1,2-hydrogen isotope shifts, commonly referred to as "NIH" shifts.[9,12] A complex of L_1 selectively labeled with deuterium at one *ortho* arene carbon (*o*-d_1-L_1) was synthesized and reacted with ^{t}BuOOH at 228 K in CH_3CN. Three phenol isotopomers were obtained on the basis of the ^1H NMR analysis of the extracted product ligand: 27% of L_1-OH had no deuterium; 23% retained deuterium in the position adjacent to the hydroxyl group (H_m'); 50% retained deuterium on the unmodified *ortho* carbon. Parallel experiments using mass spectrometry indicated 67(1)% total deuterium retention. Thus, the deuterium label induces no net isotope effect in the hydroxylation reaction. However, 46% of labilized deuterium was found on the adjacent carbon, so this system does exhibit a significant NIH shift. The intramolecular nature of this shift was confirmed by reaction of a 1:1 mixture of L_1 and d_5-L_1 complexes, which gave no crossover to mixed isotopomeric products.

2-Methyl-1-phenyl-2-propyl hydroperoxide (MPPH) is often substituted for ^{t}BuOOH to determine the course of O–O bond

(54) (a) Nam, W.; Valentine, J. S. *J. Am. Chem. Soc.* **1993**, *115*, 1772. (b) Bernadou, J.; Meunier, B. *Chem. Commun.* **1998**, 2167.

Scheme 5

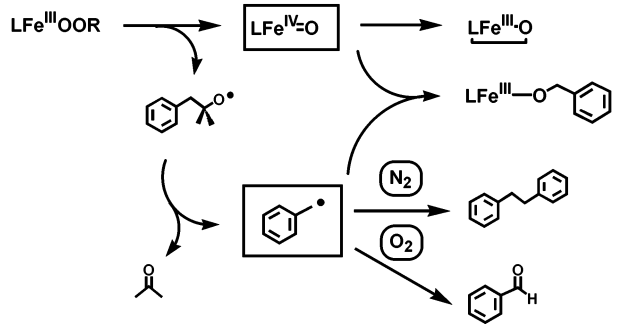

cleavage in metal-catalyzed reactions, particularly for cases where homolysis may occur.[30] Within the context of the present study, homolysis of iron(III) alkylperoxo intermediates would generate a transient alkoxy radical (RO•) that undergoes a fast (10^8 s^{-1}) β-scission to yield acetone (Scheme 5).[30] This reaction converts the oxidizing alkoxy radical into a reducing benzyl radical, which can rebound with the oxoiron(IV) coproduct to produce benzyl alcohol.[22] On the other hand, mechanisms of Fe^{III}−OOR decomposition not involving alkoxy radial formation, such as direct hydroxylation by the iron(III) alkylperoxo intermediate or O−O bond heterolysis, would generate the corresponding 2-methyl-1-phenyl-2-propyl alcohol as the byproduct.

Reaction of pure MPPH (3.0 mM) with $[(L_1)Fe^{II}(NCCH_3)_2]^{2+}$ (1.0 mM) in CH_3CN at 228 K under anaerobic conditions yielded the rebound product benzyl alcohol (1.9 mM), the benzyl radical coupling product bibenzyl (0.2 mM), and benzaldehyde (0.4 mM). No 2-methyl-1-phenyl-2-propyl alcohol was found among the products, even though control experiments verified that it was readily detectable. The product solution was yellow, and only a trace of phenolate complex was observed by UV−visible spectroscopy ($A_{780\ nm} = 0.15$ or ca. 10% yield). A ^1H NMR spectrum of the extracted product ligands showed a preponderance of unmodified 6-PhTPA (90%). On the other hand, when the reaction was carried out in the presence of O_2 under ambient pressure, a dark blue solution was obtained with $A_{780\ nm} = 1.17$, corresponding to 90% spectrophotometric yield of $[(L_1O^-)Fe^{III}(NCCH_3)]^{2+}$. Benzaldehyde (2.4 mM) was the only observed product derived from MPPH. These product distributions show that benzyl radical forms in the reactions, and this provides valuable insight into the hydroxylation mechanism (vide infra).

Discussion

On the basis of the results discussed above, a consistent mechanism of arene hydroxylation in $[(L)Fe^{II}(NCCH_3)_2]^{2+}$ complexes can be proposed. The first step involves the one-electron oxidation of the precursor iron(II) complex by ROOH to an Fe^{III}−OOR intermediate that can be stabilized and observed at 228 K. The iron(III) alkylperoxo species was characterized by a visible LMCT band, resonance enhanced Raman vibrations, and EPR signals. When the samples are left to stand, the peroxo charge-transfer band was observed to bleach, coincident with the appearance of a stable phenolate chromophore for L_1−L_5 and L_8. Thus, arene hydroxylation must be coupled to breakdown of the peroxo intermediate.[29]

Two types of reaction mechanisms are usually invoked to rationalize iron-catalyzed oxygen transfer from peroxides: free radical initiation (i.e., Haber−Weiss chemistry, Scheme 6) and electrophilic substitution by metal-centered oxidants (Scheme 7).[21,22,55] Our observations would appear incompatible with free radical chemistry. The radical most likely to form under the reaction conditions is *tert*-butoxyl (^{t}BuO•). Aromatic hydrogen abstraction by ^{t}BuO• is strongly disfavored on thermodynamic grounds, as indicated by the respective bond dissociation enthalpies of ^{t}BuO−H (105 kcal/mol)[56] and C_6H_5−H (113 kcal/mol).[57] Addition to the phenyl ring, while plausible, is nonetheless unprecedented and does not lead to phenol by any obvious path.[27,58] Moreover, the ^{18}O isotope labeling experiments clearly indicate that the phenolic oxygen is derived quantitatively from the terminal oxygen of ^{t}BuOOH. Production of hydroxyl radical (HO•) by an unrecognized process (i.e., Fenton chemistry)[59] would lead to arene hydroxylation, but such chemistry is marked by low efficiency and regioselectivity.[60] Furthermore, the efficiencies of radical-initiated arene hydroxylations are improved by the presence of oxidants that trap the cyclohexadienyl radical adducts, particularly O_2.[61] In contrast, the chemistry described here is indifferent to the presence of O_2 and is characterized by intrinsically high efficiency and absolute selectivity for *ortho* substitution, even between specific rotamers in the case of L_2. Oxygen atom transfer from unstable ^{t}BuOO• also would be consistent with the isotope labeling experiments, but again this course is without precedent and offers no obvious means to obtain the observed selectivity.

Scheme 6

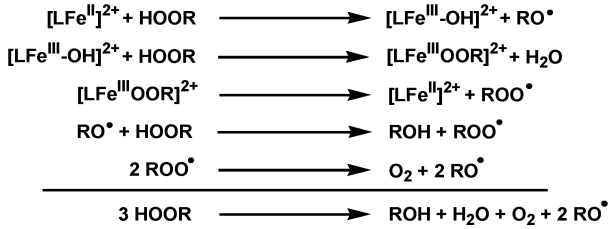

Scheme 7

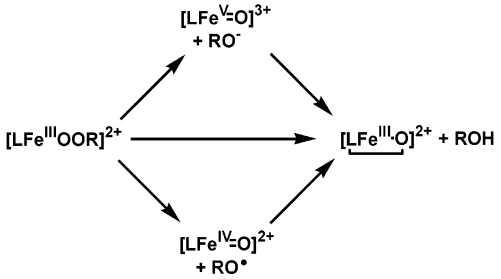

On the other hand, the exhibited efficiency and *ortho* selectivity of arene hydroxylation observed for these complexes

(55) (a) Minisci, F.; Fontana, F.; Araneo, S.; Recupero, F.; Banfi, S.; Quici, S. *J. Am. Chem. Soc.* **1995**, *117*, 226. (b) Sawyer, D. T.; Sobkowiak, A.; Matsushita, T. *Acc. Chem. Res.* **1996**, *29*, 409. (c) Walling, C. *Acc. Chem. Res.* **1998**, *31*, 155.
(56) Roth, J. P.; Yoder, J. C.; Won, T.-J.; Mayer, J. M. *Science* **2001**, *294*, 2524.
(57) Davico, G. E.; Bierbaum, V. M.; DePuy, C. H.; Ellison, G. B.; Squires, R. R. *J. Am. Chem. Soc.* **1995**, *117*, 2590.
(58) Ménage, S.; Vincent, J.-M.; Lambeaux, C.; Fontecave, M. *J. Mol. Catal., A* **1996**, *113*, 61.
(59) (a) Jefcoate, C. R. E.; Lindsay Smith, J. R.; Norman, R. O. C. *J. Chem. Soc. B* **1969**, 1013. (b) Blair, J. A.; Pearson, A. J. *J. Chem. Soc., Perkin Trans. 2* **1975**, 245. (c) Walling, C.; Johnson, R. A. *J. Am. Chem. Soc.* **1975**, *97*, 363. (d) Hage, J. P.; Llobet, A.; Sawyer, D. T. *Bioorg. Med. Chem.* **1995**, *3*, 1383.
(60) Kurata, T.; Watanabe, Y.; Katoh, M.; Sawaki, Y. *J. Am. Chem. Soc.* **1988**, *110*, 7472.
(61) (a) Dorfman, L. M.; Taub, I. A.; Buehler, R. E. *J. Chem. Phys.* **1962**, *36*, 3051. (b) Narita, N.; Tezuka, T. *J. Am. Chem. Soc.* **1982**, *104*, 7316. (c) Kunai, A.; Hata, S.; Ito, S.; Sasaki, K. *J. Am. Chem. Soc.* **1986**, *108*, 6012.

Scheme 8

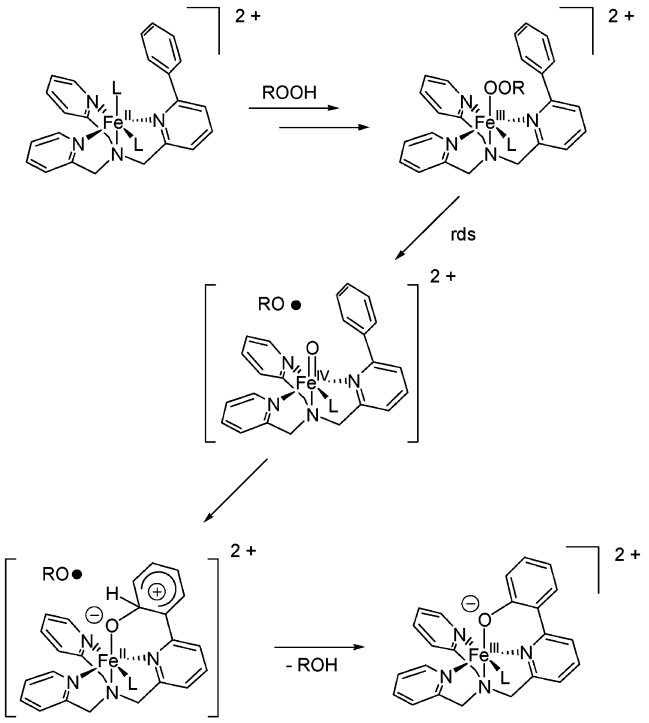

are fully consistent with a mechanism involving intramolecular electrophilic attack by a metal-centered oxidant derived from an iron(III) alkylperoxo intermediate, Schemes 7 and 8. Indeed, the geometric disposition of the aryl substituent is ideal for electrophilic *ortho* addition of a metal-centered hydroxylating agent. Crystal structures of $[(L_1)Fe^{II}(NCCH_3)_2]^{2+}$ and $[(L_6)Fe^{II}(OTf)_2]$ reveal that respective rotations about the *ipso* bonds of 48(2) and 34(3)° place the proximal *ortho* carbons at distances of 3.50 and 3.39 Å from the chelated iron(II) ions, which already approach values of 28(1)° and 2.96 Å found in the product complex, $[(L_1O^-)_2Fe_2(O)]^{2+}$. Moreover, peroxide-derived ligands coordinated trans to the amine would be exposed to the arene face, so that very little structural reorganization would be required to form an electrophilic adduct between the metal-based oxidant and the arene.[62] This geometry also would disfavor competitive N-dealkylation of the amine by H-atom abstraction from methylene positions.

Scheme 7 illustrates three options for the metal-based electrophilic attack, depending on whether O−O bond cleavage and oxygen atom transfer are concerted or stepwise. The former case involves direct attack of the iron(III) alkylperoxo intermediate on the arene, resulting in transfer of the terminal oxygen atom to a proximal *ortho* carbon. Stepwise pathways involve prior O−O bond homolysis to form oxoiron(IV) and $RO^{\bullet}$ or O−O bond heterolysis to form oxoiron(V), followed by an electrophilic addition to the arene. The results obtained from the use of MPPH as a mechanistic probe argue strongly for a path involving O−O bond homolysis. The concerted and O−O bond heterolysis pathways are excluded to the extent that 2-methyl-1-phenyl-2-propyl alcohol fails to accumulate as a reaction product. Furthermore, large yields of products derived from benzyl radical demonstrate that alkoxy radicals must form during the reaction via O−O bond homolysis of MPPH and then undergo facile β-scission. In the absence of O_2, the benzyl radical reacts readily with the homolytic oxoiron(IV) coproduct to afford benzyl alcohol, effectively quenching the arene hydroxylation. However, interception of the incipient benzyl radical by O_2 redirects the product toward benzaldehyde and preserves the oxoiron(IV) intermediate for attack on the pendant arene.

The ^{18}O isotope labeling experiments are fully consistent with the homolytic mechanism. The reaction of $^tBuO^{18}OH$ with $[(L_1)Fe^{II}(NCCH_3)_2]^{2+}$ clearly demonstrates that the terminal oxygen atom ends up on the phenolate. Furthermore, the transferred oxygen atom is susceptible to exchange with exogenous water.[54] These observations are uniquely consistent with a high-valent iron-oxo species as the reactive arene hydroxylation intermediate, presumably oxoiron(IV) generated by homolytic O−O bond cleavage of the Fe^{III}−OOR complex (Scheme 8). While the MPPH experiments demonstrate that the oxidant is a true long-lived intermediate on the diffusion time scale, its lifetime must be short relative to that of the iron(III) alkylperoxo species, and accumulation to the point of direct experimental detection was not obtained.

Although no specific role is ascribed to the homolysis coproduct $^tBuO^{\bullet}$ in the mechanism shown in Scheme 8, maximum spectrophotometric yields (87% yield of $[(L_1O^-)Fe^{III}]^{2+}$) are obtained with 1.5 equiv of ^tBuOOH (Figure 5). This stoichiometry corresponds to 0.5 equiv for the initial oxidation of iron(II) and 1.0 equiv to form the Fe^{III}−OOR intermediate and requires significant conservation of the oxidizing equivalent represented by $^tBuO^{\bullet}$. Clearly this potent oxidant can react with various species in the reaction mixture, including the iron(II) precursor complex and the iron(II) phenolate product initially obtained from the attack of the Fe^{IV}=O oxidant on the pendant aryl group.

A further interesting complexity of the observed chemistry is the accumulation of Fe^{III}−OOR intermediates as spin isomers, as demonstrated for L_1. As established for the prototypical TPA and 6-Me_3TPA complexes,[28] the spin state of the iron(III) alkylperoxo intermediate is controlled by α-substitution of the ancillary 2-pyridylmethyl arms; $[(TPA)Fe^{III}OOR]^{2+}$ is low spin, the 6-Me_3TPA analogue is high spin, and 6-MeTPA supports both low- and high-spin complexes (Table 4).[30] Correspondingly, a mixture of low- and high-spin Fe^{III}−OOR complexes also was found for L_1 in this study and only the high-spin isomer for L_8. An organonitrile solvent also supports the low-spin state, and $[(L_1)Fe^{II}(OTf)_2]$ yields only a high-spin Fe^{III}−OOR intermediate in CH_2Cl_2.

The spin isomers of iron(III) alkylperoxo intermediates are distinguished readily by characteristic resonance Raman spectra (Table 4), which were the subjects of normal coordinate analysis.[52] These analyses found that the low-spin isomer exhibits relatively stronger Fe−O bonding at the expense of a weaker O−O bond. DFT calculations on simple $(NH_3)_4Fe^{III}(OH)(OOR)^+$ models suggested a specific Fe−O d−π σ bonding interaction operant only in the low spin isomer. The conclusion that such bonding facilitates O−O bond homolysis in the low-spin iron(III) alkylperoxo isomer to form low-spin oxoiron(IV) and $RO^{\bullet}$ is supported by considerable experimental evidence that $[(TPA)Fe^{III}OOR]^{2+}$ utilizes such a decomposition path-

(62) (a) Rathore, R.; Hecht, J.; Kochi, J. K. *J. Am. Chem. Soc.* **1998**, *120*, 13278. (b) Reed, C. A.; Fackler, N. L. P.; Kim, K.-C.; Stasko, D.; Evans, D. R.; Boyd, P. D. W.; Rickard, C. E. F. *J. Am. Chem. Soc.* **1999**, *121*, 6314. (c) Hubig, S. M.; Kochi, J. K. *J. Org. Chem.* **2000**, *65*, 6807. (d) Vasilyev, A. V.; Lindeman, S. V.; Kochi, J. K. *New. J. Chem.* **2002**, *26*, 582.

way.[22] The calculations indicated a much higher barrier to O−O bond homolysis in the high-spin isomer, so that decomposition instead crosses over to homolysis of the Fe^{III}−OOR bond,[52] as noted experimentally for a series of $[(6\text{-}Me_3TPA)Fe^{III}(OOR)(O_2CR)]^+$ complexes.[63]

Such arguments might lead one to expect that decomposition of the mixed-spin Fe^{III}−OOR intermediate supported by L_1 in CH_3CN would exhibit chemistry distinct from the high-spin intermediates obtained from L_1 in CH_2Cl_2 and L_8 in CH_3CN. However, *ortho* hydroxylations of the pendant arene were obtained in all cases, the main difference being a ca. 10^3-fold faster reactivity for L_1 vs L_8 (i.e., $\Delta\Delta G^{\ddagger} = 4 \pm 1$ kcal/mol). The similar reactivities strongly suggest the high-spin isomer of Fe^{III}−OOR is a reactive precursor toward arene hydroxylation. Indeed, the high-spin isomer can be invoked as the sole productive intermediate by assigning to the low-spin Fe^{III}−OOR isomer an indirect decomposition pathway via a spin transition.

The question remains how this simple, albeit counterintuitive, mechanism might be reconciled with the previous work. The compelling experimental evidence for preferential O−O bond homolysis in low-spin Fe^{III}−OOR species derives only from studies of unsubstituted $[(TPA)Fe^{II}(NCCH_3)_2]^{2+}$ [22] and related computational studies.[52,64] The 6-phenyl substituent introduces steric interactions that are clearly evident in the ground spin state of the iron(II) complexes. The low-spin forms of the iron(III) alkylperoxo intermediates and the putative oxoiron(IV) oxidant are likely to suffer greater destabilizations due to increased steric interactions resulting from the smaller radii of the higher-valent metal ions. For example, both iron centers adopt low-spin configurations in dimeric $[(TPA)_2Fe^{III}Fe^{IV}(O)_2]^{3+}$ but are high spin in $[(6\text{-}MeTPA)_2Fe^{III}Fe^{IV}(O)_2]^{3+}$.[65] If the putative $[(6\text{-}PhTPA)Fe^{IV}(O)]^{2+}$ accordingly were to favor a high-spin state ($S = 2$), then a significant kinetic barrier would be introduced for O−O bond homolysis of the low-spin ($S = 1/2$) $[(6\text{-}PhTPA)Fe^{III}OOR]^{2+}$ intermediate compared to the high-spin ($S = 5/2$) isomer. More experimental work is necessary to substantiate this speculation.[29]

Independent of the mechanistic details of the O−O bond cleavage, it is clear that the resultant oxoiron(IV) species can effectively hydroxylate pendant aryl groups with ring substituents ranging from CH_3O to NO_2. The present results differ from those of the best studied biomimetic iron-catalyzed arene hydroxylation system thus far, which utilized a different tetradentate ligand, ethylenediamine *N*,*N*′-diacetic acid, with *N*-(3,4,5-trimethoxybenzyl) substituents.[18,19] In that study, efficient hydroxylation of the electron-rich arene was observed when the iron(III) complex was treated with either H_2O_2 or O_2/ascorbate. The use of $H_2{}^{18}O_2$ or $^{18}O_2$/ascorbate resulted in complete retention of isotope label in product phenols. In contrast to our isotope labeling results for the 6-PhTPA system, the isotope incorporation was fully preserved when the reaction was performed in normal water, and the reaction with normal isotopomeric oxidants in $H_2{}^{18}O$ yielded product without incorporated isotope. The divergent observed behaviors may simply reflect ligand-dependent effects on the kinetics of solvent water exchange of the oxoiron(IV) moiety, but involvement of distinct hydroxylating species cannot be excluded. Among the several biomimetic iron-catalyzed arene hydroxylations reported thus far,[17−19] the 6-PhTPA system is the only instance for which there is indirect evidence implicating an oxoiron(IV) oxidant.

Important arene hydroxylations in biology include those catalyzed by mononuclear nonheme iron enzymes in the metabolism of aromatic amino acids.[2,6] These enzymes utilize biopterin as a reducing cosubstrate to activate dioxygen and catalyze the hydroxylation of namesake substrates (i.e., phenylalanine, tyrosine, and tryptophan) (Scheme 1; vide supra), via a proposed oxoiron(IV) species.[9] The mechanistic details for the generation of the putative oxoiron(IV) species in the 6-PhTPA system differ significantly from those proposed for the pterin-dependent enzymes, namely O−O bond homolysis of an Fe^{III}−OOR species (Scheme 8) versus O−O bond heterolysis of an Fe^{II}−OOR species (Scheme 5). Thus, the insights we have gleaned for mechanistic steps leading to formation of the oxoiron(IV) species in the model system do not necessarily bear on the enzymatic mechanism. However, we do find evidence for the participation of an oxoiron(IV) species in the model arene hydroxylations, and this species engenders an NIH shift like that observed for the pterin-dependent hydroxylases, which has served as the hallmark for such enzymes. Our biomimetic studies thus support the involvement of an oxoiron(IV) oxidant in the mechanisms of the pterin-dependent hydroxylases.

Acknowledgment. This work was supported by a research grant (GM33162), a postdoctoral fellowship (S.J.L., GM19289). and a predoctoral traineeship (M.P.M., GM08700) from the National Institutes of Health. The crystal structure determinations were performed at the X-ray Crystallographic Laboratory of the Department of Chemistry at the University of Minnesota, under the direction of Dr. Victor G. Young, Jr. The structure solutions of $[(L_1)Fe^{II}(NCCH_3)_2](ClO_4)_2$ and $[(L_1O^-)_2Fe^{III}_2(\mu_2\text{-}O)](BPh_4)_2$ were obtained by Dr. Victor G. Young, Jr., and the structure solutions of $[(L_6)Fe^{II}(OTf)_2]$ and $[(L_8)Fe^{II}(OTf)_2]_2$ were done by Dr. Neil Brooks and William W. Brennessel, respectively. E.L.Q. is grateful for a Bather Family Undergraduate Research Fellowship.

Supporting Information Available: Tables of ^1H NMR data for free ligands L_1−L_8 (Table S1) and their iron(II) complexes (Table S2), a table of resonance Raman bands observed for phenolate chromophores (Table S3), a ^1H NMR spectrum of $[(L_1O^-)_2Fe^{III}_2(O)]^{2+}$ in CD_3CN (Figure S1), UV−visible spectra of species observed in reaction of $[L_1Fe^{II}(OTf)_2]$ in CH_2Cl_2 (Figure S2), resonance Raman spectra of $[(L_1)Fe^{III}(OOtBu)]^{2+}$ (Figure S3) and $[(L_1O^-)Fe^{III}]^{2+}$ (Figure S4) chromophores in frozen CH_2Cl_2, and X-ray crystallographic details of $[(L_6)Fe^{II}(OTf)_2]$ and $[(L_8)Fe(OTf)_2]_2$ as a separate file in CIF format. This material is available free of charge via the Internet at http://pubs.acs.org.

JA028478L

(63) Kim, J.; Zang, Y.; Costas, M.; Harrison, R. G.; Wilkinson, E. C.; Que, L., Jr. *J. Biol. Inorg. Chem.* **2001**, *6*, 275.
(64) Bassan, A.; Blomberg, M. R. A.; Siegbahn, P. E. M.; Que, L., Jr. *J. Am. Chem. Soc.* **2002**, *124*, 11056.
(65) (a) Dong, Y.; Que, L., Jr.; Kauffmann, K.; Münck, E. *J. Am. Chem. Soc.* **1995**, *117*, 11377. (b) Dong, Y.; Fujii, H.; Hendrich, M. P.; Leising, R. A.; Pan, G.; Randall, C. R.; Wilkinson, E. C.; Zang, Y.; Que, L., Jr.; Fox, B. G.; Kauffmann, K.; Münck, E. *J. Am. Chem. Soc.* **1995**, *117*, 2778.